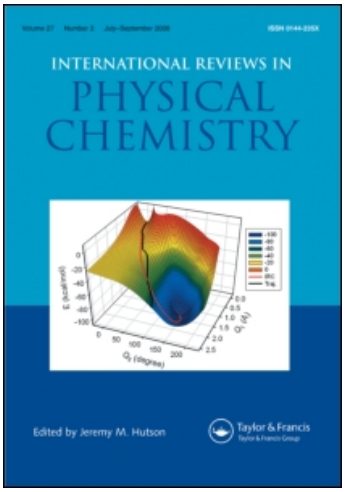

International Reviews in Physical Chemistry
Publication details, including instructions for authors and subscription information:
http://www.informaworld.com/smpp/title~content=t713724383

A model system for the study of structure and dynamics of molecules on surfaces: CO on NaCl(100)

G. E. Ewing[ab]
[a] Department of Chemistry, University of Cambridge, Cambridge, UK [b] Department of Chemistry, Indiana University, Bloomington, IN, USA

To cite this Article Ewing, G. E.(1991) 'A model system for the study of structure and dynamics of molecules on surfaces: CO on NaCl(100)', International Reviews in Physical Chemistry, 10: 4, 391 — 425
To link to this Article: DOI: 10.1080/01442359109353263
URL: http://dx.doi.org/10.1080/01442359109353263

INTERNATIONAL REVIEWS IN PHYSICAL CHEMISTRY, 1991, VOL. 10, NO. 4, 391–426

A model system for the study of structure and dynamics of molecules on surfaces: CO on NaCl(100)

by G. E. EWING†

Department of Chemistry, University of Cambridge,
Lensfield Road, Cambridge CB2 1EW, UK

In this review we describe CO on NaCl(100) as a model system for the exploration of surface structure and vibrational energy flow patterns. The system has been studied by a wide variety of surface science techniques in recent years. Thermodynamic measurements reveal the surface bond strength and polarized infrared spectroscopy demonstrates that the CO axis is perpendicular to the (100) face. Infrared photometry provides the radiative rate of the vibrationally excited CO monolayer on NaCl(100). Temperature-dependent bandshape measurements contain information on the dephasing rate. Several experiments in which the monolayer is vibrationally excited by a laser yield the phonon relaxation rate and provide an upper limit on the photodesorption rate. Infrared fluorescence from the excited monolayer has been monitored. The bond strength measurements, structure determinations, infrared band profile studies and the mapping of *all* the vibrational relaxation channels of CO on NaCl(100) comprise an unusually complete catalogue of experimental results. These results are used to test theoretical models that calculate structure and bonding, spectroscopic bandshapes and relaxation rates—with mixed success. CO on NaCl(100) appears unique among surface systems in that it is accessible to a wide variety of experimental explorations. Some of the theoretical models seem quantitatively reasonable but others, which may be qualitatively correct, need further development.

1. Overview

1.1. *Why study CO on NaCl(100)?*

Knowledge of the structures of layers adsorbed to well-defined surfaces has been evolving for many decades. The methods and results of these investigations are sufficiently matured that discussions have reached the textbook level (Adamson 1990, Somorjai 1981, Zangwill 1989). By contrast, an understanding of the dynamics of energy flow from surface bound molecules to their substrates is more primitive. Indeed it was not until 1990 that the first time-domain measurements of vibrational relaxation from an absorbed molecule to a well-defined surface were reported (Harris *et al.* 1990, Beckerle *et al.* 1990, Guyot-Sionnest *et al.* 1990 and Chang *et al.* 1990a). Dynamics measurements of the previous decade were largely confined to the analysis of band profiles as described for example in recent reviews (Gadzuk 1987, Chabal 1988, Ryberg 1989).

As data on structures and dynamics of absorbed molecules is accumulating there is a concomitant development of theoretical models that attempt to explain the results. There is the need to understand the factors that give rise to a particular structure or favour a certain relaxation pathway. It seems reasonable that this understanding is more likely to be won for those systems whose bonding arrangements are simpler.

The structures and lattice dynamics of alkali halide crystals follow naturally from considerations of the electrostatic forces of the constituent ions (Pauling 1960, Kittel 1986). There is no need to evoke chemical bonding in accounting for many physical

† Present address: Department of Chemistry, Indiana University, Bloomington, IN 47405, USA.

0144-235X/91 $3·00

properties of these crystals. Likewise, as we shall see, the bonding of molecules to the surface of alkali halide substrates is largely governed by electrostatics. The complications of conduction electrons, band gaps and electron exchange which enter discussions of bonding to metals and semiconductors (Bortolani *et al.* 1990) is unnecessary for describing the physisorbed bond that holds a small molecule to an alkali halide surface.

In answer to the question that begins the section, we have chosen CO on NaCl(100) because of the simplicity of its bonding. Other small molecules or other alkali halides could also have been selected for study and will indeed be the subjects of future research. The choice of CO on NaCl(100) was particularly fortunate since the research to be described in this review has provided not only structural details but also a complete mapping of the vibrational relaxation pathways.

The review begins with a section entitled *structure* which considers the nature of the CO and NaCl(100) surface bond. Spectroscopic consequences of this structure are also explored. In the *dynamics* section channels for vibrational relaxation are explored both by experimental and theoretical approaches. Finally, in the *afterword* we suggest directions for further research for structure and dynamics of small molecules on alkali halide surfaces.

2. Structure

Here we begin with properties of the NaCl(100) surface to which CO can attach itself. The description starts with a microscopic view of the ions at the surface and proceeds to a macroscopic perspective that considers the character of surface imperfections. The theoretical factors that determine the arrangement of CO molecules to the (100) surface and the strength of the physisorbed bond are examined. Bonding within the CO monolayer is also explored. Spectroscopic experiments in the infrared are then reviewed. An exciton model that treats the collective vibrations within the CO monolayer on the NaCl(100) surface is developed. Theoretical spectra generated from this model are then compared with the experimental results. Finally, the photometric aspects of the spectroscopic experiments are compared with theoretical models that treat the changes in oscillator strength by the adsorption process.

2.1. *The surface*

Cubes of high purity single crystal NaCl, of a size convenient to the experimentalist, are available from a variety of suppliers. Fresh surfaces of a crystal can be exposed by aligning a sharp blade, with its plane parallel to one of the side cube faces, and tapping it gently with a hammer. With practice rectangular crystals of the desired size can be produced by this cleaving process. It is the faces of cleaved crystals, placed in an ultrahigh vacuum chamber, that serve as substrates for the adsorption studies we shall describe.

At the molecular level these are (100) faces as represented in the model of figure 1. The arrangement of the ions reflects the face-centred cubic structure of the macroscopic cube as reviewed by Pauling (1960) or Kittel (1986). The ionic radius of Cl^- at 181 pm is almost twice that of Na^+ at 95 pm. The lateral separations of the ions at the surface are shown by He scattering experiments to mimic those of the bulk (Benedek *et al.* 1983). Recent atomic force microscopy (AFM) measurements on NaCl(100) support this picture (Meyer and Amer 1990a, b). In these remarkable experiments a stylus, drawn over a crystal in a UHV chamber, responds to its surface corrugation. As shown in the bottom half of figure 2, the optical display which tracks the AFM stylus picks out the

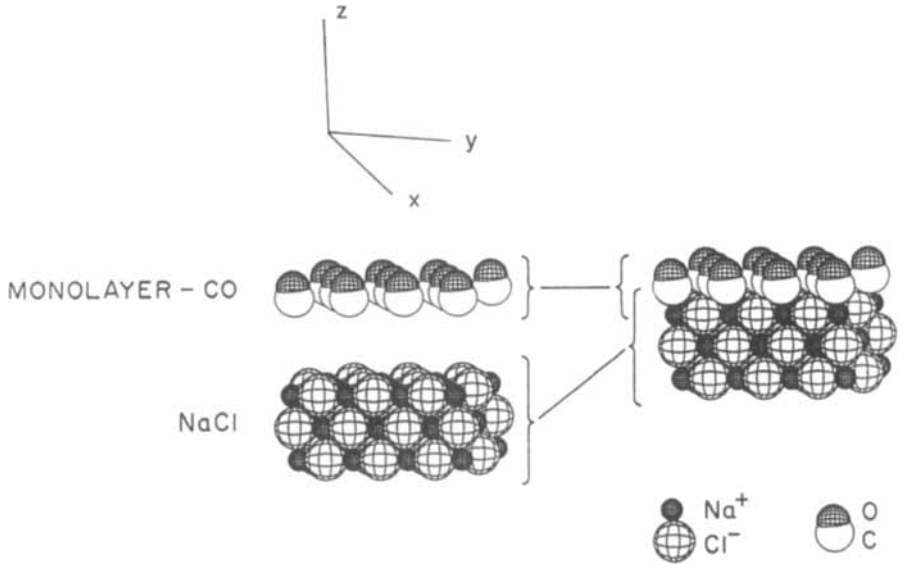

Figure 1. A model of the structure of NaCl and CO monolayer. The portion of the figure on the left has the monolayer lifted from the NaCl substrate to better illustrate the separation of the molecules and ions. The right figure portion shows CO nested on to a NaCl(100) face. The ionic and van der Waals radii are from Pauling (1960).

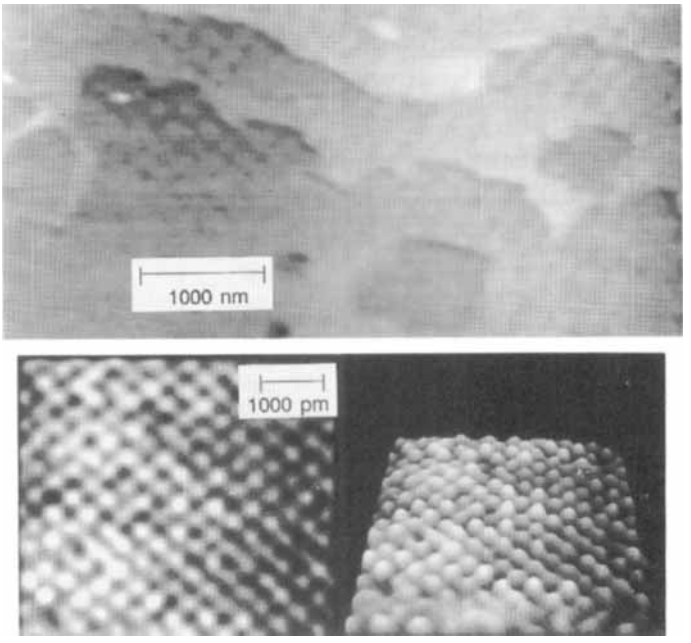

Figure 2. Atomic force microscopy of NaCl(100). The experiments are described by Meyer and Amer (1990a, b). The high resolution images on the lower portion of the figure reveal the contours of the Cl^- ions at the surface, shown in top view to the left and in perspective on the right. The ridges on the low resolution scan, in the upper half of the figure, are due to steps. These AFM scans were supplied by Dr N. M. Amer.

Cl^- ions since they are larger than the Na^+ ions. A top view of the (100) surface is shown to the left and a perspective which reveals the vertical corrugation displacement of the Cl^- ions by ≈ 50 pm.

The Na^+ ions are drawn towards the interior by 10 pm when the surface is formed according to recent calculations by Yanagihara *et al.* (1989). The Cl^- ion is displaced away from the interior by a much smaller amount. In addition to these ionic displacements, referred to as rumpling of the surface, the electrical properties of the ions are also altered. Induction effects produce a dipole in the surface Cl^- ions of 0·8 D ($2{\cdot}6 \times 10^{-30}$ Cm) directed away from the interior and a much smaller dipole in the Na^+ ions pointing in the opposite sense.

Some defects on NaCl(100) such as steps, kinks and vacancies are mechanically introduced by the cleavage process and Yanagihara *et al.* (1989) direct their attention to calculation of the relaxation of the ions at the surface in response to these imperfections. Fowler and Tole (1988) show that the polarizability of the ions in the interior of the crystal, while considerably smaller than the gas phase ions, is only slightly affected when the ions occupy sites on the (100) plane or at a step.

Some chemistry at the surface is also possible. If the crystals are let stand at elevated temperatures in moist air for several hours some Cl^- ions can be replaced by OH^- ions. This exchange has been detected by secondary ion mass spectroscopy (SIMS) in the work of Estel *et al.* (1976). However, NaCl crystals placed in an ultrahigh vacuum (UHV) chamber, within an hour of air cleavage and followed by mild bakeout, revealed no evidence of OH^- at the surface by X-ray photoelectron spectroscopy (Hardy *et al.* 1985) consistent with the SIMS study.

At the macroscopic level air cleavage of NaCl produces flat regions (terraces) interrupted by steps of atomic dimensions every 100 nm or so. This was first shown in the work of Bassett (1958). Here the cleaved salt surface was placed in a vacuum chamber and exposed to a low pressure of gold vapour. The gold atoms tend to nucleate at steps, kinks or other surface defects. The gold which has thus decorated the NaCl surface was lifted off by a film of carbon and examined by transmission electromicroscopy (TEM). Screw dislocations are thought to give rise to the spirals of different morphology (Bethge 1965). The AFM measurements of Meyer and Amer (1990b) have also revealed these steps in a low resolution scan as shown in the upper half of figure 2. Consistent with the TEM and AFM results are X-ray measurements by Kashikara *et al.* (1989) who show that the cleaved NaCl(100) face contains flat regions which differ in size and shape from one another as in a mosaic pattern.

We are left with a picture of the NaCl(100) face which is remarkably regular and *apparently* free of defects by the interrogation methods described. Regions are available for adsorption which can accommodate 10^4 to 10^5 CO molecules in terraces of the order of 100 nm on a side. We shall see spectroscopic evidence in section 2.5 consistent with this description of the surface; however, this data suggests other unidentified defects.

2.2. *Molecule-surface bonding*

Questions concerning the nature of bonding of molecules to a surface often require intricate answers. Moreover, the answers depend on whether the surface is a metal, semiconductor or an insulator (Bortolani *et al.* 1990). Fortunately, the answers appear simpler for molecular adsorption to an ionic substrate for a variety of reasons. For the case that concerns us here, the bond holding CO to NaCl(100) has a dissociation energy of $D_0 = 18\,\mathrm{kJ\,mol^{-1}}$ (Richardson *et al.* 1987a) whereas the crystal energy of NaCl is

forty times greater at 760 kJ mol^{-1} (Pauling 1960). Thus there is little reason to suppose that the presence of a monolayer of CO on NaCl(100) will significantly alter the ionic arrangement at the surface. By contrast, for CO on Pd(110) the surface geometry is reconstructed as a function of molecular coverage (Raval *et al.* 1990). Here the energy required for surface rearrangement is more nearly compatible to the energy of the bonding of the adsorbed layer and reconstruction is induced. Many adsorption bonds to semiconductors or metals are a consequence of electron exchange between the molecule and the subtrate (Bortolani *et al.* 1990). Thus the adsorption bond can have characteristics usually associated with a chemical bond. By contrast, CO and the Na^+ and Cl^- ions to which it is attached during adsorption all have closed shell configurations. Since the upper electronic states of these species are at energies much greater than the surface bond energy they are not needed to account for the adsorption process. The bonding can then be accurately described by electrostatic, induction, dispersion and repulsion forces.

Folman and his associates (Gevirzman *et al.* 1969) have made an assay of the factors responsible for the adsorption of an *isolated* CO molecule to NaCl(100) and partitioned the potential into the form

$$V(x, y, z, \alpha, \beta) = V_D + V_E + V_I + V_R, \tag{1}$$

where z describes the displacement of the centre of mass above the surface (say above the Na^+ ion) and x and y give its position in the plane of the surface. We are using the coordinate system of figure 1. The polar angles α and β (not shown) give the orientation of the CO molecular axis with respect to the z-axis and x, y plane. The Folman analysis has its origins in the discussion of adsorption of rare gases to alkali halide surfaces in the classic paper of Lennard-Jones and Dent (1928). By summing over charges of the ions of the substrate, they developed analytic expressions for the calculation of electric field and electric field gradients at any point (x, y, z) above the surface. In the treatment of CO, the electric field interacting with its dipole and the electric field gradient with its quadrupole give rise to the term V_E. The substrate generated electric field also induces a dipole in the CO through its polarizability which is then attracted to the surface and is registered by the expression V_I. Dispersion interactions between CO and ions in substrate contribute to V_D. Finally, repulsion between CO and some nearest ions yields the term V_R. By selecting a variety of sites and orientations Gevirzman *et al.* (1969) found that CO positioned vertically above Na^+ gave a minimum in the potential energy corresponding to $-V = D_e = 17\,\text{kJ mol}^{-1}$ in reasonable agreement with the estimate of $D_e = 20\,\text{kJ mol}^{-1}$ provided in the next section. The assay contains considerable uncertainty since three of the largest terms of comparable size contain different signs. The dispersion term of $V_D = -13{\cdot}7\,\text{kJ mol}^{-1}$ nearly cancels the repulsion term of $V_R = 15{\cdot}0\,\text{kJ mol}^{-1}$ and we are left with $V_E = -17{\cdot}3\,\text{kJ mol}^{-1}$ largely coming from the quadrupole interaction which one could say is responsible for the CO on NaCl(100) surface bond. It is interesting that, because of the small CO dipole moment, this electrostatic term contributes only $-0{\cdot}9\,\text{kJ mol}^{-1}$ to the surface bond in this analysis. In the electrostatic description CO sits above Na^+ rather than Cl^- because the cation is smaller than the anion (see figure 1) and allows the adsorbate to move in closer to the source charge and be bathed in a higher electric field. The vertical alignment at this site corresponds to the favourable orientation of the CO quadrupole moment in the first electric field gradient.

Calculations of Gready *et al.* (1978) of higher multipole moments of CO allowed further analysis of its bonding to NaCl(100). They also favoured the vertical alignment

of CO above Na^+ and they further show that the carbon end is down since this minimizes the octapole moment in the second gradient of the electric field producing an attractive energy of $-10{\cdot}8\,kJ\,mol^{-1}$. This structure for monolayer CO on NaCl(100) is illustrated on figure 1 where the ionic and van der Waals radii are taken from Pauling (1960). Using the CO covalent bond length of 107 pm (Herzberg 1950) these radii place the centre of mass of CO 330 pm above its underlying Na^+ ion (Chang *et al.* 1989). The nearest-neighbour separation of the CO molecules (the shortest distance between Na^+ ions) is 397 pm (Landolt-Börnstein 1955). This corresponds to a monolayer surface density of $S = 6{\cdot}3 \times 10^{14}$ molecules cm^{-2} and places the CO molecules well away from the boundaries of their van der Waals diameters as shown by figure 1.

The calculation of Gready shows that even the hexadecapole moment contributes significantly to the bonding at $-6{\cdot}2\,kJ\,mol^{-1}$. This slow convergence in the multipole interactions with the electric fields and its gradients suggests that a more realistic calculation might be achieved using distributed multipoles as described by Stone *et al.* (1985, 1988a, b).

Further refinements in understanding the nature of the bond between an isolated CO and NaCl(100) need to treat the ionic displacements at the surface of NaCl(100) and their induced charges as discussed in section 2.1. Finally, a full quantum mechanical calculation of CO together with say a small cluster of NaCl would be required to demonstrate that the expansion suggested by Gevirzman *et al.* (1969) in (1) is a realistic description of the CO on NaCl(100) bond.

Recall we have been talking about the bonding of an *isolated* CO on NaCl(100). How do the energetics change for monolayer or submonolayer coverages? Disselkamp *et al.* (1990) have addressed this question. They compare the difference in energy between an isolated CO on NaCl(100) at 330 pm above Na^+ and a full monolayer. Electrostatic interactions from dipole–dipole up to terms involving quadrupole, octapole and hexadecapole moments plus repulsion, dispersion and induced dipole-induced dipole are included in this calculation. Many cancellations occur among the nine terms they consider. The largest attractive term is dispersion at $-5{\cdot}4 \pm 0{\cdot}7\,kJ\,mol^{-1}$ and quadrupole–quadrupole interaction leads the repulsion terms at $2{\cdot}5\,kJ\,mol^{-1}$. The algebraic sum of these nine terms is $-1{\cdot}0 \pm 0{\cdot}7\,kJ\,mol^{-1}$, the large error limits coming from the uncertainty in the dispersion interaction. We see that the lateral energy within the monolayer, estimated to range from $-1{\cdot}7\,kJ\,mol^{-1}$ to $-0{\cdot}3\,kJ\,mol^{-1}$, contributes less than 10% to the estimated bond to the surface of $D_e = 20\,kJ\,mol^{-1}$.

There are yet other considerations that should be considered to complete the quantitative discussion of the energy of adsorption of a monolayer. Girard and Girardet (1988) catalogue some of these additional terms and illustrate their importance in a calculation of two molecules NH_3 on NaCl(100). They find for example that substrate-mediated dispersion remains weak with respect to multipolar induction terms. Disselkamp *et al.* (1990) have found even the induced dipole-induced dipole contribution is small within the monolayer.

In summary, the theoretical analysis of the CO on NaCl(100) molecule–surface interaction, that obviates the need for a chemical bond, has begun and the geometry implied by the minimum of the multi-dimensional potential function $V(x, y, z, \alpha, \beta)$ seems to have been located. The polarized infrared spectra described in section 2.5 is consistent with the vertical alignment of the CO molecules on NaCl(100). The strength of the surface bond of $D_e = 20\,kJ\,mol^{-1}$ as it is deconvoluted from the thermodynamic data is consistent with the theoretical analysis as are the relative weak lateral

interactions of $\approx -1\,\text{kJ mol}^{-1}$. We shall discuss these thermodynamic determinations in the next section.

2.3. *Statistical thermodynamics*

Thermodynamic measurements of CO adsorption to NaCl(100) are provided by X-ray photoelectron spectroscopy (XPS) measurements of Hardy *et al.* (1985) and Fourier transform infrared (FTIR) spectroscopy by Noda and Ewing (1990a). Both spectroscopies were used to monitor the number of CO molecules adsorbed as a function of pressure. These results for $T = 55\,\text{K}$ are summarized in figure 3 where the circles are from FTIR measurements and the squares are from the XPS study. We see essentially no further adsorption beyond 10^{-7} mbar up to 10^{-4} mbar where FTIR measurements stopped. Near 1 mbar, the vapour pressure of solid CO at 55 K (Clayton and Giauque 1932), multilayer adsorption commences. This is represented by the vertical line in figure 3. The clear demarcation of monolayer adsorption and formation of multilayer is consistent with the different values of the heats of condensation for the two phases. For monolayer adsorption the enthalpy is $\Delta H = -16 \pm 4\,\text{kJ mol}^{-1}$ (Gevirzman *et al.* 1969, Hardy *et al.* 1985, Richardson *et al.* 1987a) while condensation of the bulk solid at 55 K corresponds to $\Delta H = -8{\cdot}9\,\text{kJ mol}^{-1}$ (Clayton and Giauque 1932). This demarcation is also consistent with the qualitative difference in the electrostatic component of bonding for the two phases. The monolayer is principally drawn to the substrate by the electric fields emanating from ions while the bulk solid bonding is influenced by the much weaker molecular quadrupole interactions (Zumofen 1978). Both phases of course receive a large component from dispersion interactions.

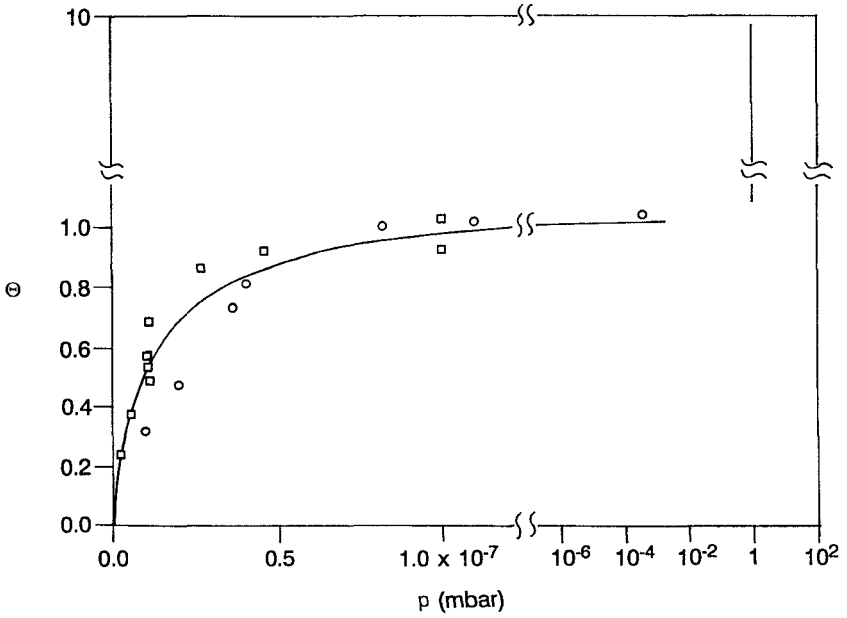

Figure 3. Isotherm for CO on NaCl(100) at 55 K. The squares are from X-ray photoelectron spectroscopy measurements and the circles from infrared photometry of the submonolayer and monolayer. The curve for the region $\Theta \leqslant 1$ is the theoretical Langmuir isotherm. The vertical line is from vapour pressure measurements of solid CO. Note change to logarithmic scale beyond 10^{-7} mbar and beyond $\Theta = 1$. Adapted from Noda and Ewing (1990).

Concentrating now on the region of submonolayer and monolayer adsorption, we can see that the experimental data are nicely fit by the theoretical isotherm of the Langmuir model (Hill 1960). This relationship, the solid curve beginning at the lower left corner of figure 3, is given by

$$\Theta(p, T)=\frac{\chi(T)p}{1+\chi(T)p}, \tag{2}$$

where Θ is the fraction of surface sites covered and p is the gas phase pressure. The effective equilibrium constant of the adsorption process is expressed by $\chi(T)$ and is temperature dependent. Near 10^{-7} mbar the surface is essentially saturated and increasing the pressure by many orders of magnitude results in no further adsorption. This saturation is the unit coverage, $\Theta=1$, and from our previous discussion every Na^+ site has a CO molecule bonded to it.

That the Langmuir relationship of (2) gives a reasonable description of the experimental results is consistent with the two assumptions of the model and the nature of the surface bonding discussed in the previous section. First, the model requires that the adsorption is localized at sites. For example, the adsorbed molecules are not allowed to skate along the surface. The specific electrostatic bonding of CO to Na^+ demonstrated by Gevirzman *et al.* (1969) and Gready *et al.* (1978) is consistent with this picture. Second, the adsorption to a particular site is unaffected by the occupation of neighbouring sites. This requirement is approximately met by the calculation of Disselkamp *et al.* (1990) which shows that lateral interaction within the monolayer at $\approx -1\,\mathrm{kJ\,mol^{-1}}$ contributes less than 10% to the total surface bond. At 55 K this contribution is about 50% of RT. For other adsorbed molecules on NaCl(100), for example CO_2, the lateral interactions are more important (Berg and Ewing 1989) and a Langmuir isotherm cannot represent the data (Heidberg *et al.* 1990c).

Statistical mechanics techniques allow the calculation of $\chi(T)$ if the bond energy D_0 and the five vibrational motions of the adsorbed molecule are known. Two of these vibrations are the frustrated translations as the adsorbed CO oscillates parallel to the surface. With x and y axes in the NaCl(100) plane these modes have frequencies $\tilde{\nu}_x$ and $\tilde{\nu}_y$. Vibrational motion perpendicular to the surface against the physisorbed bond is given by $\tilde{\nu}_z$. Finally,, frustrated rotations of CO at its absorbed site have frequencies $\tilde{\nu}_{\alpha_x}$ and $\tilde{\nu}_{\alpha_y}$. With these surface bond parameters, Hill's (1960) clear treatment gives

$$\chi(T)=q_{\mathrm{ads}}(T)\exp(D_0/\mathrm{RT})/q_{\mathrm{gas}}(T) \tag{3}$$

with the gas phase partition function expressed by

$$q_{\mathrm{gas}}(T)=\left[\left(\frac{2\pi mkT}{h^2}\right)^{3/2}\frac{kT}{p^0}\right]\frac{0{\cdot}695\,T}{B}, \tag{4}$$

where all terms in (4) are in SI units except for the rotational constant $B=1{\cdot}9\,\mathrm{cm^{-1}}$ (Herzberg 1950). The CO mass is m and h and k are Planck's and Boltzmann's constant, respectively. The standard state pressure is taken at $p^0=1$ Pa (0·01 mbar). The absorbed molecule partition function is given by

$$q_{\mathrm{ads}}(T)=\prod_{i=1}^{5}[1-\exp(-hc\tilde{\nu}_i/kT)]^{-1}, \tag{5}$$

where c is the speed of light and the five vibrational frequencies against the surface, $\tilde{\nu}_i=\tilde{\nu}_1$ to $\tilde{\nu}_5$ ($\tilde{\nu}_x, \tilde{\nu}_y, \tilde{\nu}_z, \tilde{\nu}_{\alpha_x}, \tilde{\nu}_{\alpha_y}$), are assumed harmonic.

Measurements of $\chi(T)$ at a variety of temperatures are not sufficient to uniquely establish the six parameters D_0, $\tilde{\nu}_1, \ldots \tilde{\nu}_5$. Some information of the surface bond frequencies is available from other measurements. Gevirzman *et al.* (1969) use the shape of the potential function of (1) to estimate a value of $\tilde{\nu}_z = 90\,\mathrm{cm}^{-1}$. Richardson *et al.* (1987a) find the frustrated rotational frequencies to be $\tilde{\nu}_{\alpha_x} = \tilde{\nu}_{\alpha_y} = 140\,\mathrm{cm}^{-1}$ from an infrared combination band. Finally, the dephasing measurement described in section 3.1 suggests a value of $\tilde{\nu}_x = \tilde{\nu}_y \approx 40 \pm 5\,\mathrm{cm}^{-1}$ for the frustrated translation. In order to fit the adsorption isotherm parameter of $\chi(T) = 1 \times 10^6\,\mathrm{Pa}^{-1}$ ($1 \times 10^8\,\mathrm{mbar}^{-1}$) from the $T = 55$ K data of figure 3, use of these values of $\tilde{\nu}_i$ and (3) to (5) requires $D_0 = 18\,\mathrm{kJ\,mol}^{-1}$ or

$$D_e = D_0 + 1/2 \sum_{i=1}^{5} hc\tilde{\nu}_i = 20\,\mathrm{kJ\,mol}^{-1}.$$

This value of D_e is comparable with the theoretical estimate of this value of $17\,\mathrm{kJ\,mol}^{-1}$ given in the previous section using (1). Moreover, use of standard statistical mechanics expressions (Richardson *et al.* 1987a) allows the calculation of enthalpy of adsorption from equation (3) and is found to be $\Delta H = -19\,\mathrm{kJ\,mol}^{-1}$ at 55 K. This is within the wide experimental error limits of $\Delta H = -16 \pm 4\,\mathrm{kJ\,mol}^{-1}$ from the work of Gevirzman *et al.* (1969), Hardy *et al.* (1985) and Richardson *et al.* (1987a).

In summary the Langmuir model, and the accompanying statistical mechanics it implies, can account for the adsorption of CO on NaCl(100) based on the available thermodynamic data. It should be noted, however, that this thermodynamic data admit wide error limits. Since CO on NaCl(100) serves as a model for physisorption we feel that the thermodynamics of this important system needs a more accurate examination to provide a stringent test of the Langmuir model and the nature of the surface bond.

2.4. *Infrared spectroscopy*

The first studies of infrared spectroscopy of CO on NaCl used a film consisting of crystallites as the substrate (Gevirzman *et al.* 1969). The film, produced by sublimation, is a loosely packed arrangement of nearly regular cubes mimicking the morphology of single crystals of the bulk material. The crystallites are, however, small with edge lengths of the order of 10 to 100 nm (Richardson *et al.* 1987a) and the concentration of defects on the surface could be considerable. As a consequence, the infrared adsorption of CO on these films reveals a diffuse asymmetric profile with bandwidth (fullwidth at half maximum) of $\Gamma \approx 10\,\mathrm{cm}^{-1}$, reflecting the heterogeneity of the surface. By contrast, the bandwidth of CO on NaCl(100) single crystal can be two orders of magnitude smaller (Disselkamp *et al.* 1990). However, no matter how the substrate is prepared, the bandcentre of CO adsorbed on to NaCl is near $2155\,\mathrm{cm}^{-1}$ and shifted less than 1% from its gas phase value at $2143\,\mathrm{cm}^{-1}$ (Herzberg 1950). Thus the surface bond has a trivial influence on the CO chemical bond force constant.

Richardson and Ewing (1987b) and Heidberg *et al.* (1987a) were first to explore the NaCl(100) single crystal spectroscopy of adsorbed CO. An UHV chamber and optical arrangement for these types of experiments is sketched in figure 4. Two air cleaved NaCl crystals are mounted to a copper cryogenic work surface that can provide temperatures to 5 K. The four exposed surfaces are available for adsorption as the chamber is supplied with gaseous CO at the appropriate pressure. The interrogating infrared radiation can be polarized either E_p as shown or E_s (out of the plane of the figure). The propagating light vector makes an angle θ with the z-axis.

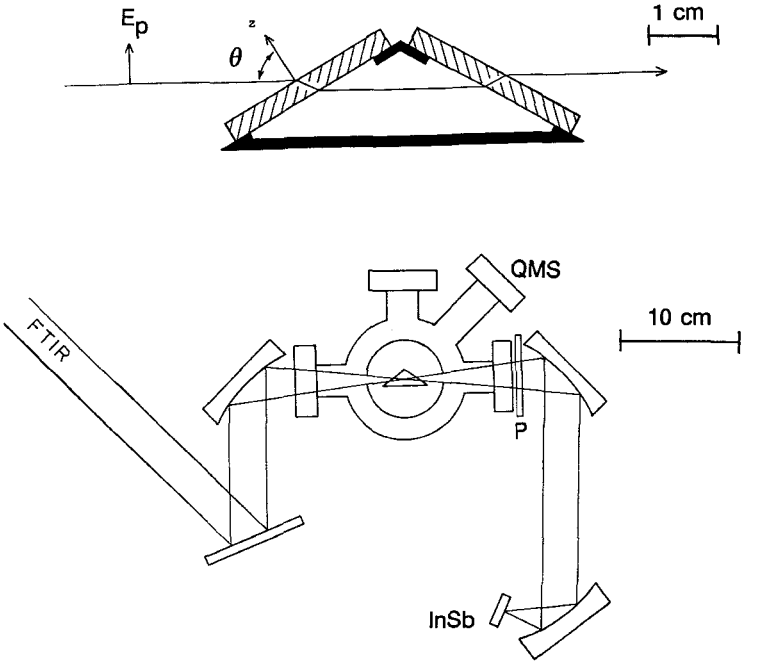

Figure 4. The UHV chamber and optical schematic. The lower portion of the figure shows the chamber. Transfer optics carry radiation from the Fourier Transform Infrared (FTIR) interferometer through two optical ports, a polarizer (P), and on to a InSb detector. These two ports were also used for the laser induced desorption experiment. The upper port was used for laser access in the laser induced fluorescence measurements. The fourth port opens to a quadrupole mass spectrometer (QMS). The upper portion of the figure shows an enlarged view of the salt crystals (cross-hatched) and their relationship to E_p polarized light. Four surfaces are available for adsorption. Adapted from Richardson *et al.* (1987b).

Spectra at 55 K for coverages from $\Theta = 0{\cdot}3$ to 1·0 (Noda and Ewing 1990) are shown in figure 5. The interrogating polarization was E_p, allowing the oscillating electric field to couple with the transition dipole of the CO molecules aligned along the z-axis (see figure 4). No absorption was observed when the adsorbed layer was examined with E_s polarization, since in this case the electric field of the radiation is orthogonal to the CO bond axis. These polarization measurements are consistent with the structure of the CO monolayer shown in figure 1.

Pressures dictated by figure 3 were used to control the submonolayer coverages. At $\Theta = 1{\cdot}0$ the band profile is symmetric with bandwidth $\Gamma = 0{\cdot}42\ \text{cm}^{-1}$. As the coverage is lowered the band broadens, becomes asymmetric and shifts to higher wavenumber. The growing diffuseness and shift as the coverage is reduced is consistent with the random arrangement of CO molecules on the available sites as required in the Langmuir model. By contrast for submonolayer CO_2, the bandwidth and band position does not change with coverage (Berg and Ewing 1989). Here the molecules group into islands. The environment of any CO_2 is much the same as any other and the islands produce similar spectra.

By pumping away the surrounding CO gas while lowering the temperature of the substrate, the monolayer can be studied at lower temperatures. (The multilayer spectra

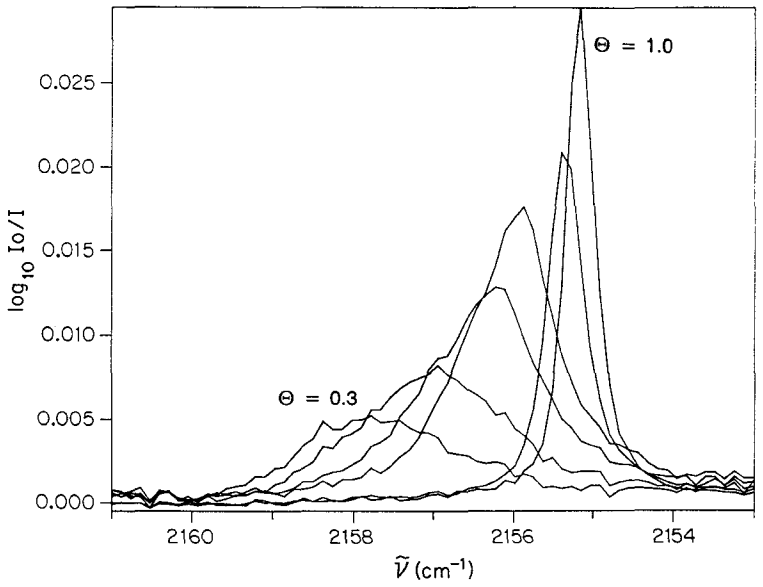

Figure 5. The coverage dependence of the CO on NaCl(100) absorption profile. The system temperature is 55 K. The diffuse features between $\Theta = 0{\cdot}3$ and $\Theta = 1{\cdot}0$ are intermediate coverages on NaCl(100). The absorbance for the lowest four coverages have been scaled by a factor of two. For equilibrium CO pressures at these coverages see figure 3. Taken from Noda and Ewing (1990).

of CO on NaCl(100) have also been examined by Chang *et al.* (1988). These features are well removed from the monolayer features and will not be discussed in this review.) Spectra for $\Theta = 1$ CO on NaCl(100) are shown in figure 6 for three temperatures (Chang *et al.* 1990). The bandwidths sharpen and shift to lower wavenumber as the temperature is lowered. Below 10 K no further change in the band profile or position occurs. The bandshapes for samples 20 K and above are symmetric and well represented by a Lorenztian profile as we show in figure 7 for $T = 55$ K. We shall be discussing the significance of these spectroscopic changes at the higher temperatures in section 3.1.

At the lowest temperatures $\leqslant 10$ K the bandshape is no longer symmetric. This is emphasized in figure 8 from the data of Disselkamp *et al.* (1990) where an empirical fit with a Gaussian profile (the dotted curve) is attempted. A distinct shoulder appears displaced $0{\cdot}1\ \mathrm{cm}^{-1}$ to lower wavenumber of the bandcentre. The bandwidth of the central feature $\Gamma \approx 0{\cdot}07\ \mathrm{cm}^{-1}$ (corrected for instrument resolution) is the narrowest reported for *any* surface bound molecule. As we shall show in section 3, the relaxation lifetime below 10 K is 4·3 ms. This lifetime would correspond to a Heisenberg limited bandwidth of $10^{-9}\ \mathrm{cm}^{-1}$. Why then is the bandwidth at $0{\cdot}07\ \mathrm{cm}^{-1}$ so *broad* and what is the origin of the shoulder in figure 8?

Disselkamp *et al.* (1990) have explored the possible origin of the band position and band profile of the observed low temperature spectrum of CO on NaCl(100). They pose the question: what is the spectrum of a layer of CO molecules that might fit into one of the large terraces bounded by steps such as those shown in figure 2? The answer to the question was found by generating theoretical spectra of arrays containing many molecules. The model is the exciton description of condensed phase spectroscopy discussed for example by Craig and Walmsley (1963).

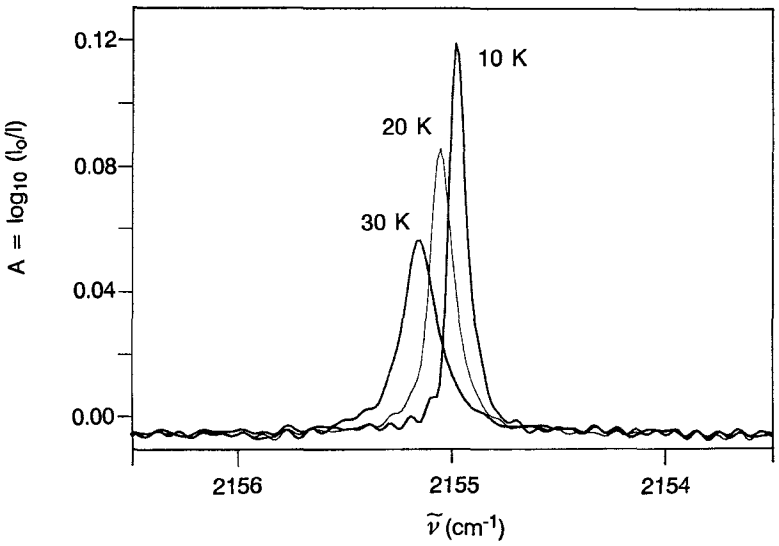

Figure 6. Infrared absorption of monolayer CO on NaCl(100) at various temperatures. The CO has been depleted in ^{13}C and is principally $^{12}C^{16}O$. Adapted from Chang *et al.* (1990).

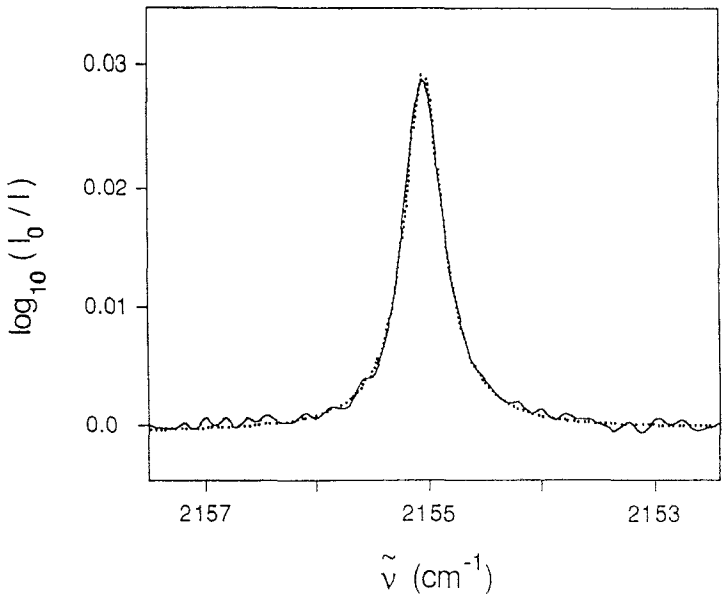

Figure 7. Absorbance of a monolayer of CO on NaCl(100) with E_p polarization. The sample temperature is 55 K and the pressure of CO in the chamber is 1×10^{-5} mbar. The solid curve is the experimental data and the dotted curve is a Lorentzian profile. Taken from Richardson *et al.* (1989).

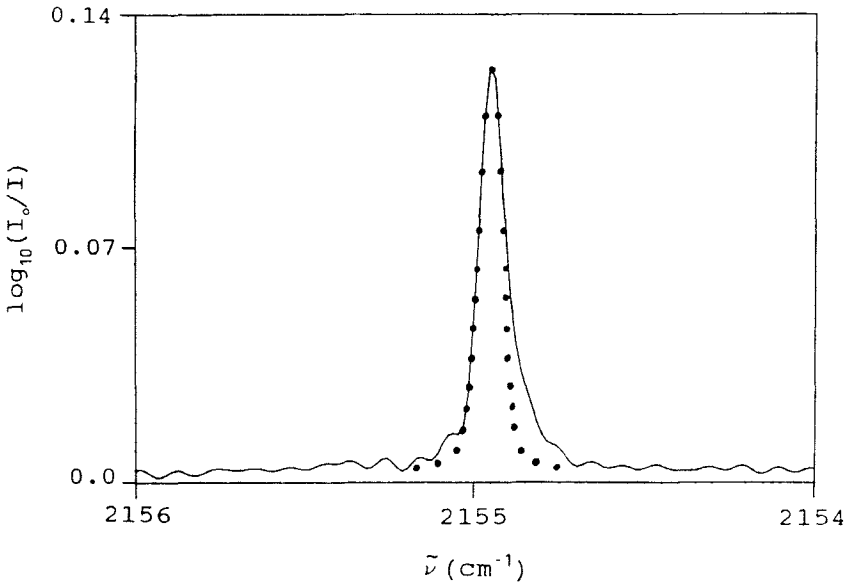

Figure 8. Infrared absorbance of monolayer CO on NaCl(100). The absorbance at 5 K is shown by the solid curve. A Gaussian profile, given by solid circles, is offered for comparison. Notice the asymmetry in the lower energy region of the observed bandshape. Taken from Disselkamp *et al.* (1990).

Vibrational motions for N molecules are coupled through the Hamiltonian,

$$\hat{H}' = \sum_{i}^{N}\sum_{j<1}^{N}\left\{\frac{\mu_i\mu_j}{R_{ij}^3} - \frac{3}{2}(\mu_i\Omega_j + \mu_j\Omega_i)\left(\frac{1}{R_{ij}^5}\right) + \frac{9}{4}\left(\frac{\Theta_i\Theta_j}{R_{ij}^5}\right) - \frac{75}{16}(\Theta_i\Phi_j + \Theta_j\Phi_i)\left(\frac{1}{R_{ij}^7}\right) + \frac{25}{4}\left(\frac{\Omega_i\Omega_j}{R_{ij}^7}\right) + \frac{1225}{64}\left(\frac{\Phi_i\Phi_j}{R_{ij}^9}\right) + \ldots\right\}, \tag{6}$$

where μ, Θ, Ω and Φ are the dipole, quadrupole, octapole, and hexadecapole moments, respectively and R_{ij} is the separation distance between molecules i and j. Higher order electric multipole terms were not included due to the lack of available data. The importance of such terms, which may converge slowly, is not known. The zeroth order wavefunctions chosen to describe a two dimensional array of monolayer CO were written as

$$\psi_0(v=0) = \varphi_1, \varphi_2, \varphi_3 \ldots \varphi_N \tag{7a}$$

$$\psi_m(v=1) = C_{m,1}\varphi_1'\varphi_2, \varphi_3 \ldots \varphi_N + C_{m,2}\varphi_1, \varphi_2'\varphi_3 \ldots \varphi_N + C_{m,3}\varphi_1, \varphi_2, \varphi_3' \ldots \varphi_N + \ldots + C_{m,N}\varphi_1, \varphi_2, \varphi_3 \ldots \varphi_N', \tag{7b}$$

where φ_1, φ_2, φ_3,... φ_N are the ground state orthonormal anharmonic oscillator vibrational wavefunctions for molecules 1, 2, 3,... N and $C_{m,1}$, $C_{m,2}$,... $C_{m,N}$ are the coefficients of the zeroth order wavefunction of quantum state m, ranging from 1 to N, to be determined. The primed notation signifies one quantum of vibrational excitation whereas the unprimed notation implies that the molecule is in its ground state. The ground state wavefunction of (7 *a*) and the first excited state wavefunctions of (7 *b*) together with the perturbation Hamiltonian of (6) give rise to a 1 × 1 and N × N secular determinant, respectively. Since the array is a collection of identical molecules, only a

small number of matrix elements for CO are needed. Actually, three matrix elements for each electric multipole moment are required. As an example, the dipole moment matrix elements for molecule j are written as

$$\langle\varphi'_j|\mu_j|\varphi'_j\rangle = \mu_j^{11}$$
$$\langle\varphi_j|\mu_j|\varphi_j\rangle = \mu_j^{00}$$
$$\langle\varphi_j|\mu_j|\varphi'_j\rangle = \mu_j^{01} \tag{8}$$

where μ_j^{11} and μ_j^{00} are the permanent dipole moments averaged over $\upsilon=1$ and $\upsilon=0$, respectively, and μ_j^{01} is the transition dipole moment between the $\upsilon=0$ and $\upsilon=1$ states. The first two matrix elements of (8) have traditionally been referred to as static matrix elements, in the sense that the vibrational averaging takes place over one vibrational state. The last term of (8) is referred to as a dynamic matrix element. It involves the transition between two vibrational states. Values for all the matrix elements were obtained from the literature. To apply the perturbation Hamiltonian of (6) and set-up the secular determinant, the appropriate matrix elements were selected and weighted by the monolayer structure separation distances raised to the appropriate power. The results of the secular determinant calculation are vibrational frequencies and wavefunctions.

A vibrational frequency in a domain is denoted by $\tilde{\nu}_m^{(N)}$, where N gives the domain size and m is the eigenstate of the vibrational excited level as in (7*b*). The perturbation treatment here actually yields the frequency shifts $\Delta\tilde{\nu}_m^{(N)} = \tilde{\nu}_m^{(N)} - \tilde{\nu}_1^{(1)}$, where $\tilde{\nu}_1^{(1)}$ is the isolated and therefore uncoupled (i.e. $\hat{H}'=0$ in (6)) vibrational frequency of the CO molecule absorbed on to NaCl(100). It was not possible to determine $\tilde{\nu}_1^{(1)}$ from the calculation, but it was obtained from extrapolation of experimental results such as those shown in figure 5 and estimated to be $2159\,\mathrm{cm}^{-1}$ for $^{12}C^{16}O$. With these definitions, the integrated cross-section for a given domain were calculated. By using the perturbed transition frequencies of CO for a domain containing N molecules, $\Delta\tilde{\nu}_m^{(N)}$, the experimental value of $\tilde{\nu}_1^{(1)}$, and excited state wavefunctions ψ_m, Disselkamp *et al.* (1990) calculated the integrated cross-sections (cm molecule^{-1}) for each quantum state m using

$$\bar{\sigma}_m(N) = \frac{8\pi^3\tilde{\nu}_m^{(N)}}{Nhc}|\langle\psi_m|\sum_{j=1}^{N}\mu_j|\psi_0\rangle|^2 \tag{9}$$

appropriate for aligned transition dipoles (Chang and Ewing 1989). It is important to notice that whereas perturbations within the adsorbate involve many electric multipole terms, as (6) reveals, the integrated cross-section is only determined by the electric dipole operator. The integrated cross-section calculation used here, based on the oriented gas model, has ignored the attenuating influence of induction effects which we shall discuss in the following section.

Some spectra that were calculated for square domains are shown in figure 9. At $N=576$ two features (the solid lines) are apparent. For 576 coupled oscillators we expect 576 frequencies. Some are degenerate because of the symmetry of the chosen square array. However, very few of the transitions have any appreciable intensity. The dominant feature about $0{\cdot}6\,\mathrm{cm}^{-1}$ to the high frequency of $\Delta\tilde{\nu}_m^{(N)}=0{\cdot}0\,\mathrm{cm}^{-1}$ corresponds to in-phase vibration of all 576 oscillators. A weaker transition, about $0{\cdot}4\,\mathrm{cm}^{-1}$ below $\Delta\tilde{\nu}_m^{(N)}=0{\cdot}0\,\mathrm{cm}^{-1}$ corresponds to an out-of-phase vibration. The hundreds of other transitions, which have oscillator strength, are too weak to appear on the cross-section scale of figure 9. For $N=2500$ the dominant feature has moved to slightly

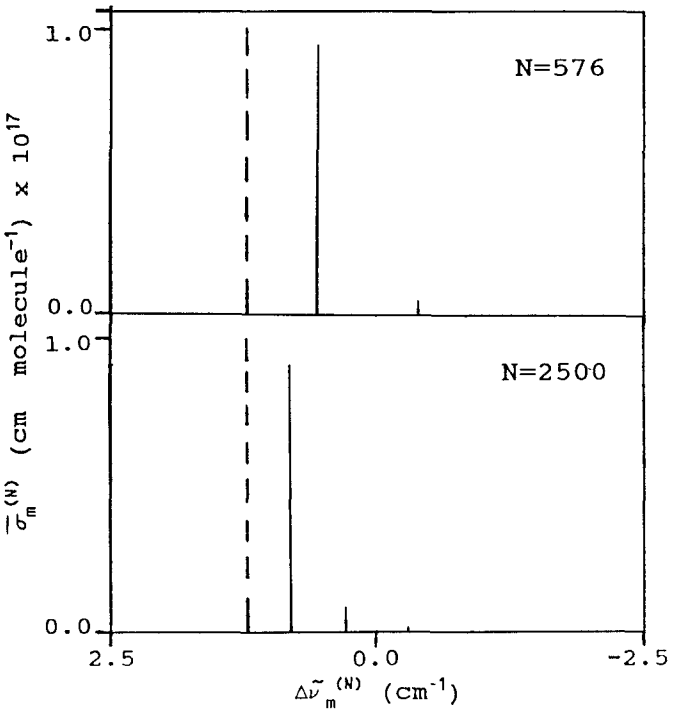

Figure 9. The integrated cross-section $\bar{\sigma}_m^{(N)}$ for square domains of CO containing 576 and 2500 molecules is represented. The dashed vertical line indicates the calculated result for the infinite monolayer. Adapted from Disselkamp *et al.* (1990).

higher frequency. The weak low frequency satellite has moved closer to the main feature. A very weak feature, to the low wavenumber side of $\Delta\tilde{\nu}_m^{(N)} = 0{\cdot}0\,\text{cm}^{-1}$, is also barely visible in figure 9. It is possible to calculate analytically the limiting frequency of the monolayer described by the Hamiltonian of (6) for $N \to \infty$ since the lattice sums are available (van der Hoff *et al.* 1953). For the infinite monolayer the satellites of the finite domains collapse on to the single absorption feature. This feature is shown in figure 9 by the dashed line. The calculation of the finite domain spectra beyond $N = 2500$ (which took one week on a 8820 DEC VAX) is not practical. However, extrapolation of the satellite feature to $N \sim 10^5$ give its separation from the dominant absorption at $\approx 0{\cdot}1\,\text{cm}^{-1}$ consistent with the shoulder observed in the data of figure 8.

Thus there is a plausible explanation for the structure of the absorption of CO on NaCl(100) at low temperature. The shoulder is a consequence of the boundaries of the finite domain of CO molecules. The estimate, $N \sim 10^5$, is comparable to the number of CO molecules that could fit into a square island bounded by the $\sim 100\,\text{nm}$ step separation in figure 2. Since the frequency of the central feature is domain size-dependent, as shown by the calculation results of figure 9, each island will have a slightly different absorption spectrum. The resulting spectrum of the $\sim 1\,\text{cm}^2$ area sampled by the infrared probe to produce figure 8 is a convolution of a mosaic of CO monolayer islands. This heterogeneity could account for the observed diffusiveness giving the bandwidth of $\Gamma \approx 0{\cdot}07\,\text{cm}^{-1}$.

While the calculation just described is quite involved, many important contributions to the Hamiltonian of equation (6) have been neglected. For example,

dispersion, repulsion and induction terms (analogous to V_D, V_R and V_I terms of (1)) have been ignored. Thus quantitative agreement for the size-dependent or coverage-dependent spectra are not expected.

However, the electrostatic model alone does quite well in accounting for the isotope dilution experiments of Heidberg *et al.* (1987a) and Noda and Ewing (1990). Some of these results are shown in figure 10 for $^{12}C^{16}O$ diluted by $^{13}C^{16}O$. At a $x_i = 0{\cdot}97$ mole fraction of $^{12}C^{16}O$ in $^{13}C^{16}O$ and 55 K, the Lorenztian profile is essentially the same as that for $\Theta = 1{\cdot}0$ of figure 7. As the $^{12}C^{16}O$ concentration is reduced the band shifts to shorter wavenumber, broadens and becomes skewed. (The same behaviour occurs in the $^{13}C^{16}O$ spectral region near 2106 cm^{-1} during isotope dilution.) The shift, $\Delta\tilde{\nu}$, with isotopic dilution was orginally analysed for classical oscillators by Hammaker *et al.* (1965), and further developed by Mahan and Lucas (1978) and Persson and Ryberg (1981). A simple expression has evolved:

$$\Delta\tilde{\nu} = \frac{\alpha_v U_0 x_i \tilde{\nu}_1^{(1)}}{2(1 + \alpha_e U_0 x_i)}. \tag{10}$$

The model considers coupling through the oscillation of electric dipoles (the first term in (6)). The size of the transition dipole (μ_j^{01} of (8)) is contained in the term α_v. The transition dipole induces opposition dipoles within the adsorbed layer and depends on the electronic polarizability α_e. The effect of this attenuation appears in the denominator of (10). All the dipoles (intrinsic and induced) of the monolayer are totalled by using the lattice sum U_0 which adds all the R_{ij}^{-3} terms of (6). Taking values of CO on NaCl(100) ($\alpha_v = 5{\cdot}2 \times 10^{-26}\,cm^3$, $\alpha_e = 2{\cdot}3 \times 10^{-24}\,cm^3$ and $U_0 = 0{\cdot}14 \times 10^{24}\,cm^{-3}$ from Noda and Ewing (1990)) reveals $\Delta\tilde{\nu} = 5{\cdot}9\,cm^{-1}$ from (10) for $x_i = 1$. Thus $^{12}C^{16}O$ infinitely diluted in $^{13}C^{16}O$ shifts by $+5{\cdot}9\,cm^{-1}$ when in the neat layer. Extrapolation of the data of figure 10 gives $+5{\cdot}0\,cm^{-1}$. Thus the electrostatic model does quite well.

Using the exciton model, Disselkamp *et al.* (1990) randomly placed 800 $^{12}C^{16}O$ and 800 $^{13}C^{16}O$ isotopes in a square array and calculated the spectrum. Their results in the region of the $^{12}C^{16}O$ absorption at $x_i = 0{\cdot}5$ are shown in figure 11 together with the $x_i = 0{\cdot}63$ insert from figure 10. Of the 1600 vibrational modes possible for the system, a considerable number have oscillator strength as revealed in the 'stick spectrum' of figure 11. Each line is broadened by $0{\cdot}5\,cm^{-1}$, a value comparable to dephasing contributions (section 3.1), and summed to give the calculated profile. The calculated bandcentre is in reasonable agreement with the experimental result. The degradation of the bandshape to low wavenumber and the overall bandwidth is also consistent with experiment.

Finally, let us return to the submonolayer spectra of figure 5 and explore why it is diffuse on the basis of the exciton model. We will examine the results of three computer experiments by Disselkamp *et al.* (1990). In each of the experiments they consider a surface with 1600 available sites (i.e. the Na^+ ions). In the first experiment they randomly cover half the sites with isotopically pure $^{12}C^{16}O$ with isolated molecule frequency of $\tilde{\nu}_1^{(1)} = 2159\,cm^{-1}$. The result for this computer experiment with $\Theta = 0{\cdot}5$, the top panel of figure 12, is similar to the full coverage $\Theta = 1{\cdot}0$ calculation of figure 9. Of the 800 possible transitions only one has any appreciable oscillator strength. A second transition gives rise to the weak low frequency satellite. The oscillators are so well coupled that the random arrangement of the vacancies at $\Theta = 0{\cdot}5$ still gives a simple result: a single dominant feature. Thus, the diffuseness we observe for submonolayer coverages in the spectroscopic experiments of figure 5 is *not* due to a

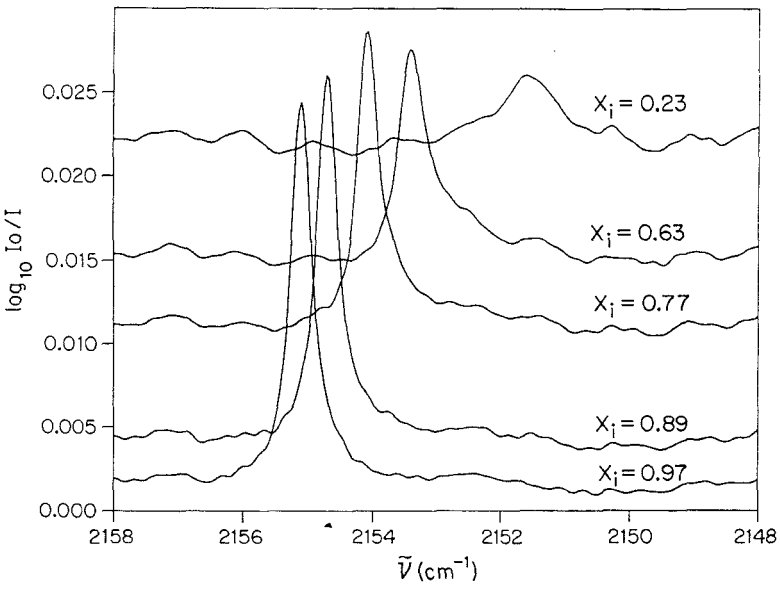

Figure 10. The mole-fraction dependence of the $^{12}C^{16}O$ absorption profiles. Here x_i refers to the mole fraction of $^{12}C^{16}O$ in $^{13}C^{16}O$. The total CO pressure was 2×10^{-6} mbar in order to maintain monolayer coverage at 55 K. Taken from Noda and Ewing (1990).

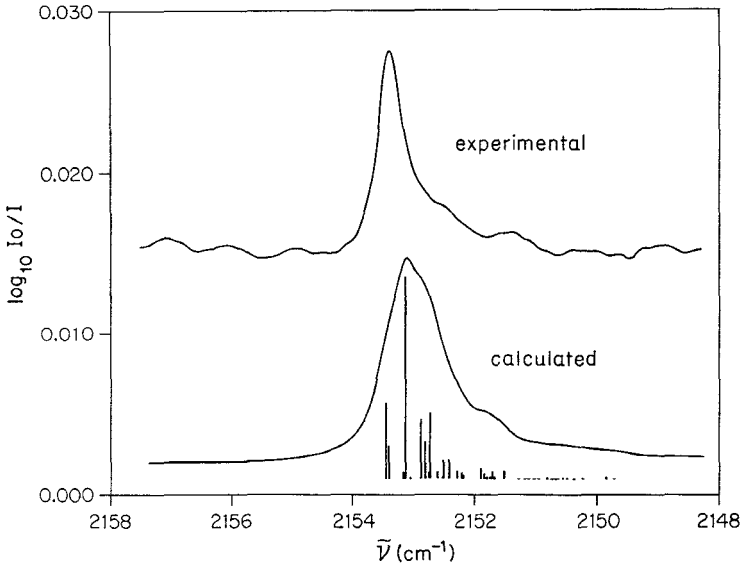

Figure 11. A comparison between experimental and calculated spectra of mixed $^{12}C^{16}O$ and $^{13}C^{16}O$ isotopes on NaCl(100) at $\Theta = 1{\cdot}0$. The upper spectrum is taken directly from figure 10 for $x_i = 0{\cdot}63$. The lower stick and broadened spectra for $x_i = 0{\cdot}50$ are adapted from Noda and Ewing (1990).

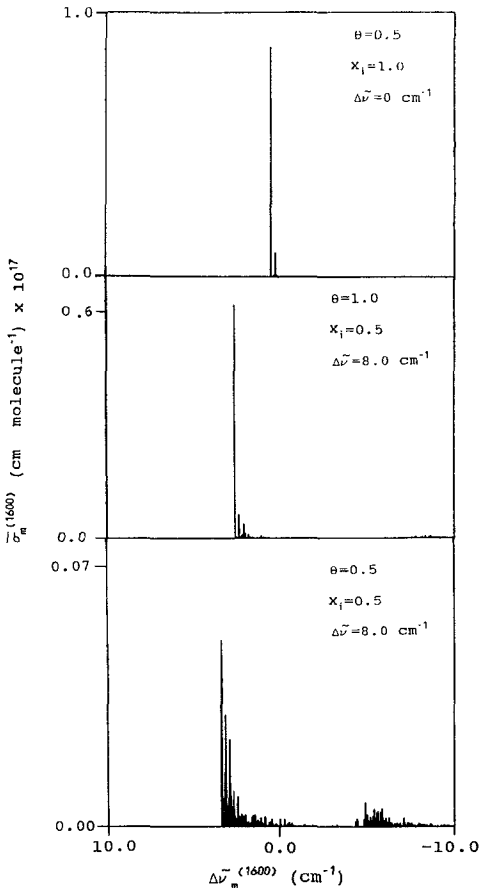

Figure 12. Calculated cross-sections of CO on NaCl(100). The upper panel is for $\Theta = 0{\cdot}3$ of neat $^{12}C^{16}O$. The calculated cross-section for a $x_i = 0{\cdot}5$ mixture of CO molecules whose vibrational frequencies differ by $8{\cdot}0\,cm^{-1}$, located about the origin in the figure by $-4{\cdot}0\,cm^{-1}$ and $+4{\cdot}0\,cm^{-1}$, is shown for a full monolayer, middle panel, and half monolayer, lower panel. Adapted from Disselkamp *et al.* (1990).

random arrangement of identical oscillators. Next Disselkamp *et al.* (1990) suppose, in the $\Theta = 0{\cdot}5$ computer experiment, that the oscillators are not identical but differ in frequency by $8\,cm^{-1}$. Half are at $2163\,cm^{-1}$ and the other half at $2155\,cm^{-1}$. This frequency separation is consistent with the difference expected for CO molecules on a smooth region of NaCl(100) and those on defective sites (Richardson *et al.* 1987a). These defects, not revealed by the AFM results of figure 2(*a*), might for example be vacancies at the surface. In the computer experiment, the lower panel of figure 12, we see a complex hash of features spread over $\approx 2\,cm^{-1}$, to higher wavenumber, and a weaker cluster of features appear at lower wavenumber. The high frequency components have borrowed most of the intensity from the low frequency components. This intensity partitioning among adsorbed molecules was first noted by Hammaker *et al.* (1965). The diffuseness of this computer spectrum is consistent with the diffuseness observed from the laboratory data of figure 5 for the submonolayer. Extending the computer experiment to full coverage, $\Theta = 1{\cdot}0$, with a random distribution of the two

distinct sites gives a single dominant feature with several very weak satellites as shown in the middle panel of figure 12. Both the shift to lower frequency and the band sharpening is consistent with the behaviour of the $\Theta = 1{\cdot}0$ feature in the laboratory experiment of figure 5. The phenomenon of band narrowing due to electrostatic coupling has recently been explored by Perrson and Ryberg (1990). Thus the sharp spectrum we observe in figure 8 is not necessarily evidence for a surface free of imperfections. Rather the calculations suggest that in order to explain both the monolayer and submonolayer experiments the surface contains defects as well as terraces bounded by occasional steps.

2.5. *Photometry*

Here we will make the connection between isolated molecule properties and the absorbance of the monolayer. This connection is possible since there is apparently no need to involve chemical forces (exchange of electrons) to account for the attachment of CO to the NaCl(100) surface.

The simplest approach toward understanding the photometry of adsorbed molecules is to treat them as an oriented gas. We follow the analysis of Richardson *et al.* (1989). They begin by considering the integrated cross-section in the gas phase molecules. A variety of measurements over the years has converged on the value $\bar{\sigma}_g = 1{\cdot}0 \times 10^{-17}$ cm molecule^{-1} (Varasani *et al.* 1975). The gas phase cross-section, σ_g (cm^2 molecule^{-1}), is contained in the Beer–Lambert law, $I_0/I = \exp(\sigma_g \rho l)$, with ρ the molecular density (molecules cm^{-3}) and l (cm) the pathlength. The transmittance of the sample is I/I_0. The absorbance, integrated over $\tilde{\nu}$ (cm^{-1}) across the band profile, then becomes

$$\tilde{A} = \int_{\text{band}} \log_{10}(I_0/I)\,\mathrm{d}\tilde{\nu} = \frac{\rho l}{2{\cdot}303} \int_{\text{band}} \sigma_g\,\mathrm{d}\tilde{\nu} = \frac{\rho l \bar{\sigma}_g}{2{\cdot}303}. \tag{11}$$

For our purpose it is important to realize that $\bar{\sigma}_g$ refers to molecules in random orientations in the gas phase and components of the transition dipole moment are shared equally among x, y and z laboratory coordinates. For the case of CO on NaCl(100) all molecules are aligned along the z-axis (see figure 1) so $\bar{\sigma}_z = 3\bar{\sigma}_g$ and $\bar{\sigma}_x = \bar{\sigma}_y = 0$.

Modifying (11) for the oriented gas phase molecules, we note $S = \rho l$ (molecules cm^{-2}) is the surface density of the adsorbed molecules. A factor of $\sin^2\theta$ gives the projection of light intensity of E_p polarization along the z-axis (see figure 4). The crystal tilted with respect to the cylinder of interrogating light offers an elliptical sampling of adsorbed molecules. This results in a factor of $\cos\theta$ in the denominator. Finally, when we have n adsorption surfaces, (11) becomes

$$\tilde{A}_p = \frac{nS\bar{\sigma}_z \sin^2\theta}{2{\cdot}303\cos\theta}, \tag{12}$$

where the subscript p reminds us that we are using E_p polarization. For the experimental arrangement of figure 4, $\theta = 60°$, $n = 4$ and with $\bar{\sigma}_z = 3\bar{\sigma}_g = 3{\cdot}0 \times 10^{-17}$ cm molecule^{-1} and $S = 6{\cdot}3 \times 10^{14}$ molecules cm^{-2} (12) gives $\tilde{A}_p = 0{\cdot}049$ cm^{-1}. The measured integrated absorbance from the data of figures 6–8, which is invariant with temperature, is $\tilde{A}_p = 0{\cdot}019 \pm 0{\cdot}002$ cm^{-1} or too small by a factor of $2{\cdot}6 \pm 0{\cdot}3$. Despite its simplicity, the oriented gas model falls short of quantitatively explaining the data.

The next level of sophistication involves solving Maxwell's equations across the boundaries of a thin film (the monolayer) on a substrate. This problem goes back to the work of Airy (1833). Richardson *et al.* (1989), Chen and Schaich (1989) supply more recent references in their discussion of the transmission experiment through a monolayer of CO on NaCl(100). The result, for crystals canted at Brewster's angle (see figure 4), is given by

$$\tilde{A}_p = \frac{nS\bar{\sigma}_z \sin^2\theta}{2{\cdot}303\cos\theta(1+U_0\alpha_e)^2}, \tag{13}$$

where the calculated integrated absorbance is now reduced by a factor $(1+U_0\alpha_e)^2$ over the oriented gas result of (12). This factor essentially includes the cancellation contribution of the induced dipoles within the monolayer. With values of U_0 and α_e given in section 2.4, (13) predicts $\tilde{A}_p = 0{\cdot}028\ \mathrm{cm}^{-1}$. The theoretical result is now 50% too high.

Chen and Schaich (1989) have considered the effect of dipoles induced in the underlying ionic substrate by the transition dipoles of the CO monolayer but the effect is very small for this system. The 50% discrepancy remains. Richardson *et al.* (1989) use an *ab initio* calculation of Bauschlicher (1985) to show that $\bar{\sigma}_z$ is reduced by 10% by the intense electric field (4×10^9 V/m) at each CO on its site above Na^+ on the (100) crystal surface. The theoretical result of (13) is then 30% higher than the observed integrated absorbance. A discrepancy of this size can be accounted for by the vibrational Stark effect (Lambert 1991).

3. Dynamics

When molecules are in thermal equilibrium with their surroundings, the population in each quantum state is dictated by the Maxwell–Boltzmann distribution. However, this does not mean the molecule will gain or lose energy and make transitions to different quantum states to maintain a dynamic equilibrium. This process is sometimes referred to as thermal exchange (or thermal scrambling). The thermal exchange occurs among the v_i low-frequency CO surface bond modes above 10 K where these levels begin to be populated. We now introduce a $v=1$ internal excitation of CO (by photon absorption) that is far from equilibrium and consider its fate. The four channels of vibrational relaxation are given by (14) to (17):

$$\mathrm{CO^*\ldots NaCl} \xrightarrow{k_{\mathrm{dph}}} \mathrm{[CO\ldots NaCl]^*} \tag{14}$$

$$\mathrm{CO^*\ldots NaCl} \xrightarrow{k_{\mathrm{rad}}} \mathrm{CO\ldots NaCl} + h\nu, \tag{15}$$

$$\mathrm{CO^*\ldots NaCl} \xrightarrow{k_{\mathrm{phn}}} \mathrm{CO\ldots NaCl^*}, \tag{16}$$

$$\mathrm{CO^*\ldots NaCl} \xrightarrow{k_{\mathrm{vid}}} \mathrm{CO + NaCl} + \Delta E. \tag{17}$$

In (14) the phase of the $v=1$ vibration, initially localized in CO* (the asterisk represents this excitation), is interrupted by motions against the surface bond (indicated by the dots). An experimental consequence of this relaxation, at rate k_{dph}, is a broadening of

the vibrational band profile and a shift in its frequency as the temperature of the system is raised. Radiation from CO* in (15) proceeds with rate k_{rad}. In (16), the vibrational excitation in CO* is transferred to the underlying substrate and phonon excitation results at rate k_{phn}. Finally since the vibrational energy of CO* exceeds the surface bond strength, photodesorption is possible and CO, now vibrationally relaxed, flies away with kinetic energy ΔE. This process, called vibrational induced desorption at rate k_{vid}, is shown in (17). Processes (15) to (17) resulting in loss of population of the vibrational excited state of CO* are associated with time T_1. Dephasing, which still maintains excitation in the vibrating chemical bond in CO, is characterized by time T_2.

The relaxation channels of (15) to (17) can, in principle, contribute to the bandwidth of the infrared absorption. However, as we shall show below, the relaxation by any of these channels is so slow that broadening of the infrared band will be negligible. Thermal exchange by contrast preserves the CO ($\upsilon = 1$) vibrational excitation, but it can significantly contribute to the bandwidth, as we shall see. We shall discuss the dephasing (T_2) process first, followed by examination of the three population relaxation channels.

3.1. *Dephasing rate:* k_{dph}

As shown in figure 6, both the position of the infrared absorption and the bandwidth of CO on NaCl(100) change with temperature. This behaviour has been noted from a variety of studies of adsorbed molecule systems as reviewed by Ryberg (1989), Chabal (1988) and Gadzuk (1987). The qualitative explanation is as follows. If the time scale of the thermal excitation (and de-excitation) processes is long compared to the lifetime of the $\upsilon = 1$ CO state due to other relaxation processes, the vibrational motion of this state will not be perturbed and the spectral bandwidth will be determined by the $\upsilon = 1$ decay. On the other hand, if the thermal excitation time scale is shorter than the lifetime of the $\upsilon = 1$ state, the vibrational motion of the excited state will be interrupted and the phase will be randomized. Band frequency shift and broadening will occur as a result of this vibrational dephasing. It will be the registry of the temperature dependence of both centre frequency and bandwidth that will demonstrate thermal exchange as the dominant relaxation mechanism. This registry is apparent from the spectra of figure 6 and its representation as band position, $\tilde{\nu}_c$, and bandwidth, Γ, in figure 13.

Noda, Richardson and Ewing (1990) have adopted the argument presented by Harris *et al.* (1977, 1978) and Shelby *et al.* (1979) for a simplified case of a high frequency mode (which is identified as the CO stretching vibration) coupled with one of the surface modes. We will distinguish the high frequency vibrational mode of CO with quantum number υ from υ_i which will represent one of the surface mode levels. It is further assumed that only the first excited level υ_i exists. The energy level diagram is shown schematically in figure 14. The frequency for the ($\upsilon = 1$, $\upsilon_i = 0$)–($\upsilon = 0$, $\upsilon_i = 0$) transition is given by $\tilde{\nu}_0$. This corresponds to the low temperature limit of the absorption frequency. The frequency for the ($\upsilon = 1$, $\upsilon_i = 1$)–($\upsilon = 0$, $\upsilon_i = 1$) transition is given by $\tilde{\nu}_0 + \delta\tilde{\nu}$, where $\delta\tilde{\nu}$ is the frequency offset for the sequence band. The energy difference between the ($\upsilon = 1$, $\upsilon_i = 1$) and ($\upsilon = 1$, $\upsilon_i = 0$) level is represented by E_i, and τ is the measure of the thermal de-excitation lifetime of the surface mode. The FWHM (in wavenumbers) is denoted by Γ and is related to a lifetime by $1/(2\pi c\Gamma)$.

For the situation described above the band profile can be well approximated by a Lorentzian as was demonstrated in figure 7 for the 55 K spectrum. The frequency (in

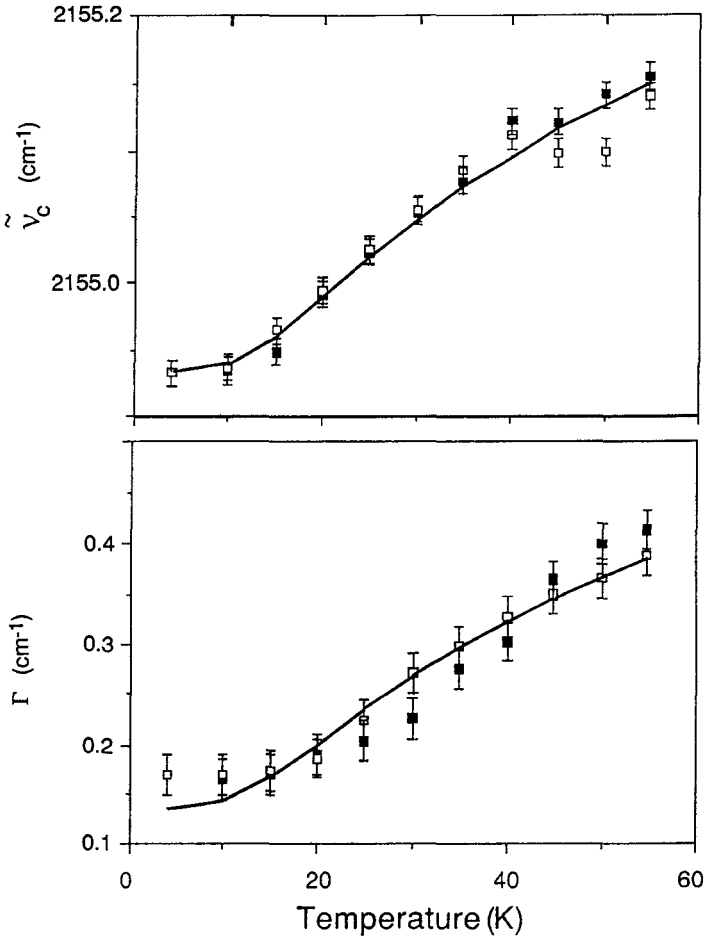

Figure 13. Temperature dependence of the frequency ($\tilde{\nu}_c$) and bandwidth (Γ) of monolayer CO on NaCl(100). Solid squares (■) and open squares (□) represent experimental data points with rising temperature and with lowering temperature, respectively. The solid lines are the best fit for the data using (18) and (19). From Noda, Richardson and Ewing (1990).

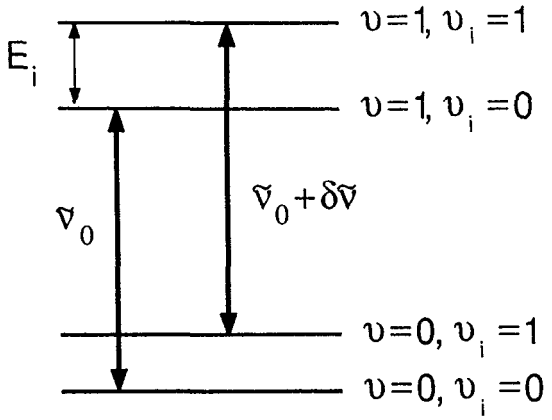

Figure 14. Schematic energy level diagram for vibrational dephasing of CO on NaCl(100). See text for definitions of symbols. From Noda, Richardson and Ewing (1990).

wavenumbers) and bandwidth dependence that follows from this model yields the simple relationships

$$\tilde{\nu}_c = \tilde{\nu}_0 + \frac{(\delta\tilde{\nu})g\exp(-E_i/RT)}{1+(2\pi c\delta\tilde{\nu})^2\tau^2}, \tag{18}$$

$$\Gamma = \Gamma_0 + \frac{(2\pi c)(\delta\tilde{\nu})^2\tau g\exp(-E_i/RT)}{1+(2\pi c\delta\tilde{\nu})^2\tau^2}, \tag{19}$$

where g gives the degeneracy of the surface mode involved in the thermal exchange.

The experimental data can be fit to (18) and (19), as figure 13 reveals. The pertinent parameters are $\tau/g = 5{\cdot}7 \pm 0{\cdot}6$ ps $(\delta\tilde{\nu})g = 1{\cdot}1 \pm 0{\cdot}1\,\mathrm{cm}^{-1}$ and $E_i = 330 \pm 40\,\mathrm{J\,mol}^{-1}$ ($\tilde{\nu}_i = 40 \pm 5\,\mathrm{cm}^{-1}$). Good agreement is apparent for both the bandwidth and the frequency shift temperature dependence. In addition, the Lorentzian band shape we observed at various temperatures are in accordance with the model. The frequency $\tilde{\nu}_i$ of $40 \pm 5\,\mathrm{cm}^{-1}$, consistent with the thermodynamic data, supports the assignment of the frustrated translational modes ($\tilde{\nu}_x$, $\tilde{\nu}_y$) as causing the vibrational dephasing. The degeneracy factor g will be 2 for this mode, and we obtain $\delta\tilde{\nu} = 0{\cdot}55 \pm 0{\cdot}05\,\mathrm{cm}^{-1}$, $\tau = 11 \pm 1$ ps or $k_{\mathrm{dph}} = 9 \pm 1 \times 10^{10}\,\mathrm{s}^{-1}$.

Despite the self-consistency of the spectroscopic features with the form of (18) and (19), we must not forget that a number of adjustable parameters have been used to fit the data. Moreover coupling among the CO molecules within the monolayer has been ignored. Coupling leads to collective vibrations, or excitons, rather than the isolated motions we have pictured, and will effect the absorption band profile and its frequency. Persson *et al.* (1986) have considered the effect of collective motions through transition dipole coupling on the dephasing process. This model works well for NO on Ni(111), as Erley and Persson (1989) show, but fails for CO on NaCl(100) according to the analysis of Noda, Richardson and Ewing (1990). What can be the difficulty with a model that has so successfully accounted for other adsorbed molecule spectroscopy? We can first note that the spectroscopic changes are much smaller for CO on NaCl(100) than for, say, NO on Ni(111). In the former case the frequency shifts by only $\approx 0{\cdot}2\,\mathrm{cm}^{-1}$, while in the later case $\tilde{\nu}_c$ changes by $\approx 5\,\mathrm{cm}^{-1}$ over the temperature range studied. We next note that the transition dipole interaction incorporated into the coupling model of Persson *et al.* (1986) may not be the dominant coupling mechanism for CO on NaCl(100). As Mahan and Lucas (1978) were careful to point out in their example of exciton shift, transition dipole coupling accounted for only one third of the observed frequency shift. In an analysis of the contributions to the frequency shift in CO on NaCl(100), Noda and Ewing (1990) found: dynamic dipole + higher multipoles + dispersion to be $+5{\cdot}9 + (-6{\cdot}6) + (-2{\cdot}7) = -3{\cdot}4\,\mathrm{cm}^{-1}$. (The experimental value is $\Delta\tilde{\nu} = -4\,\mathrm{cm}^{-1}$.)

Where the spectroscopic changes in response to vibrational dephasing are slight, as in the case of CO on NaCl(100), all the contributions to coupling that produce collective motions within a monolayer must be included before changes in $\tilde{\nu}_c$ and Γ can be adequately explained. Thus the system CO on NaCl(100) becomes a sensitive test of vibrational dephasing models and further theoretical work is required to explain the data.

3.2. *Radiative rate:* k_{rad}

If there were neither photodesorption nor relaxation into the substrate, population loss of excited vibrational levels by radiation alone would contribute to T_1 as (15) shows. Fluorescence decay would then follow the rate k_{rad}. However, as we shall soon

see, the fluorescence decay is largely determined by relaxation into phonons. We can however obtain k_{rad} without time-domain measurements. This is accomplished by first obtaining the effective integrated cross-section, $\bar{\sigma}_z$, for CO on NaCl(100) from the integrated absorbance measurement by using (12). Manipulations of standard expressions for spontaneous emission then reveal

$$k_{rad}^{1\to 0} = 8\pi c\tilde{\nu}^2\bar{\sigma}_z/3 \tag{20}$$

as shown by Chang and Ewing (1989). The result for $^{13}C^{16}O$ which we shall need shortly is found to be $k_{rad}^{1\to 0} = 11\ s^{-1}$. (The radiative rate and cross-section of the $^{12}C^{16}O$ isotope differs slightly.) This rate is about one-third that of the isolated gas phase molecule (Millikan 1963). However, as we discussed in section 2.5 the polarizability of the molecules within the monolayer are responsible for much of this reduction in the radiative rate. For arrays of $N \sim 10^5$ CO molecules on NaCl(100), the emission would be superradiant with $k_{rad} = Nk_{rad}^{1\to 0}$ *if* the vibration defining the exciton remained coherent. However since $k_{dph} \gg k_{rad}^{1\to 0}$, the coherence is scrambled by dephasing and, by arguments given by Grad *et al.* (1988), the radiative rate for monolayer CO on NaCl(100) for $T > 20$ k is correctly given by (20).

3.3. *Phonon relaxation rate:* k_{phn}

We can use the observed fluorescence decay rate k_{obs}, as a clock to evaluate the rate constants k_{phn} and k_{vid} from the relationship

$$k_{obs} = k_{rad} + k_{phn} + k_{vid}. \tag{21}$$

As we shall show in the next section, the vibrationally induced desorption rate is exceedingly small and can be neglected in the above equation. Chang and Ewing (1990a) made the fluorescence measurements by preparing a monolayer of $^{13}C^{16}O$ on NaCl(100) and cooling the system to 22 K. For this isotope and at this temperature the absorption profile embraces the $P_{1\to 0}(9)$ line of a gas phase laser line as shown in figure 15. (The laser excitation was introduced into the upper port of the UHV chamber of figure 4.) Fluorescence was captured in the first overtone ($\Delta\upsilon = -2$) region by a cooled InSb detector following excitation from pulses of the Q-switched laser. By averaging signals from 50 000 pulses, Chang and Ewing (1990a) recorded the fluorescence decay of figure 16 to obtain a time constant of 4·3 ms or $k_{obs} = 2{\cdot}3 \times 10^2\ s^{-1}$. It would *appear* that since k_{rad} was established in section 3.2 it remains only to do the simple extraction from (21) to obtain k_{phn}. However, we need to look more closely at the nature of the fluorescence experiment. In particular we must account for the observation of fluorescence in the *overtone* region, e.g. $\upsilon = 2 \to 1$, while only the $\upsilon = 1$ level was pumped by the laser.

Excitation of the CO $\upsilon = 1$ vibrational level proceeds according to

$$CO(\upsilon = 0) + h\nu \xrightarrow{k_p} CO(\upsilon = 1) \tag{22}$$

with rate constant k_p which depends on the cross-section σ_z at the frequency of the pumping laser line. This process is followed by energy pooling

$$CO(\upsilon = 1) + CO(\upsilon = 1) \leftrightarrows CO(\upsilon = 2) + CO(\upsilon = 0) + \Delta E = 23\ cm^{-1}. \tag{23}$$

The reaction is exothermic by 23 cm^{-1} due to the anharmonicity of CO. This energy pooling process can continue to high vibrational states. (Pooling up to $\upsilon = 30$ has been observed for multilayer $^{13}C^{16}O$ on NaCl(100) (Chang and Ewing 1990b)). The use of filters in the monolayer fluorescence measurements suggest excitation to about the

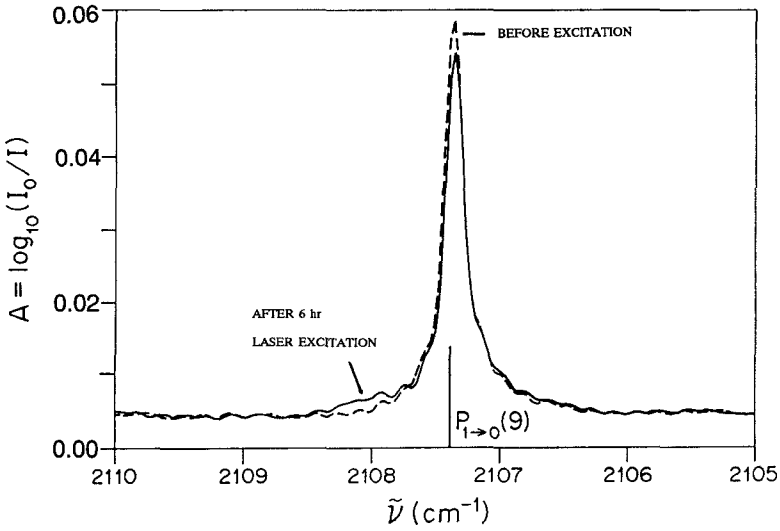

Figure 15. Comparison of vibrational spectra of monolayer $^{13}C^{16}O$ on NaCl(100) at 22 K before and after laser excitation. As described in the text, (– – –) was obtained before laser irradiation. The solid curve was obtained after 6 h of laser irradiation. The exciting CO laser line $P_{1\rightarrow0}(9)$ is indicated at the position of 2107·42 cm^{-1}. Taken from Chang and Ewing (1989).

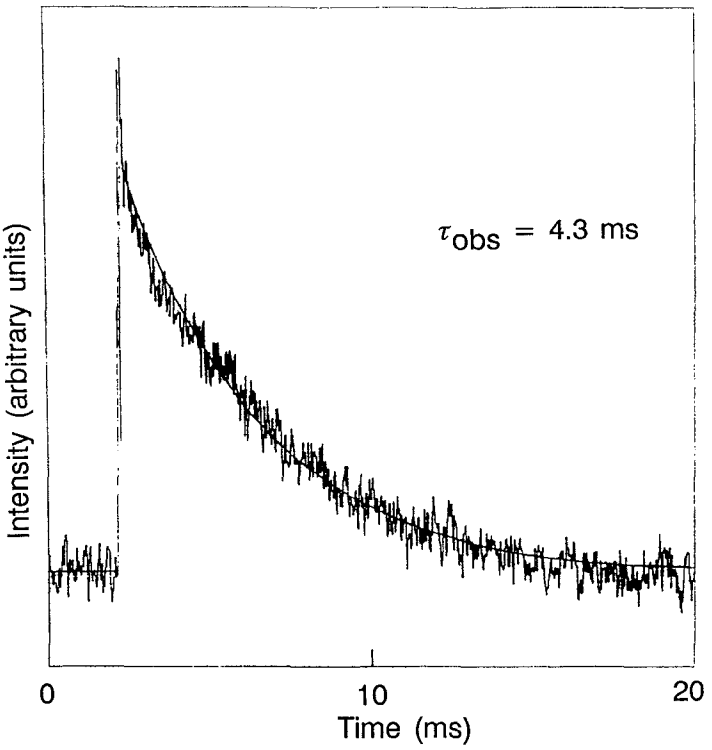

Figure 16. Time evolution of infrared fluorescence from a monolayer of vibrationally excited $^{13}C^{16}O$ on NaCl(100). The fluorescence decay can be fitted with a simple exponential function (solid curve) and has a time constant of 4·3 ms. From Chang and Ewing (1990a).

$\upsilon = 15$ level. From other studies of spontaneous emission of excited CO levels it is known that the rate increases by a factor of 10 from $\upsilon = 1$ to $\upsilon = 15$ (Legay-Sommaire and Legay 1980). Chang and Ewing (1990b) therefore scaled their measured radiation rate, $k_{\text{rad}}^{1\to 0} = 11\,\text{s}^{-1}$, by the geometric mean of this factor, $10^{1/2}$, to obtain an effective radiative rate of $k_{\text{rad}} \approx 30\,\text{s}^{-1}$. Taking $k_{\text{obs}} \approx k_{\text{rad}} + k_{\text{phn}}$, by neglecting the k_{vib} term in (21), they therefore uncovered $k_{\text{phn}} \approx 2 \times 10^2\,\text{s}^{-1}$ as an effective phonon relaxation rate for levels $1 \leqslant \upsilon \leqslant 15$.

The value of k_{phn} just determined is in agreement with the classical model developed by Chance *et al.* (CPS) (1978). Here an oscillating point dipole located at a distance z_e from the surface transmits its radiation at rate k_{rad}. The ability of the substrate, the receiver, to accept this radiation depends on the value of its complex dielectric constant. The dielectric constant at the frequency of the radiation $\tilde{\nu}$, is defined by $\hat{\varepsilon}(\tilde{\nu}) = (\eta + i\kappa)^2$ where η is the index of refraction and κ the extinction coefficient. This simple model allows easy calculation of the relaxation to phonons through

$$k_{\text{phn}} = \frac{3\eta\kappa k_{\text{rad}}}{16\pi^3 \tilde{\nu}^3 |\hat{\varepsilon}(\tilde{\nu}) + 1|^2 z_e^3}. \tag{24}$$

As before, the effective radiative rate for $1 \leqslant \upsilon \leqslant 15$ is $k_{\text{rad}} \approx 30\,\text{s}^{-1}$. The geometric mean of the $^{13}C^{16}O$ fundamental frequency in the range $\upsilon = 1$ to $\upsilon = 15$ is $\tilde{\nu} \approx 1930\,\text{cm}^{-1}$ (Herzberg 1950) and $z_e = 3{\cdot}3 \times 10^{-8}$ cm is the distance between the CO centre of mass and the centre of an Na^+ ion at the surface (Chang and Ewing 1989). From the bulk optical properties of NaCl, $\eta = 1{\cdot}52$ and $\kappa = 1{\cdot}8 \times 10^{-9}$ (Palik 1985), the result of the calculation is $k_{\text{phn}} \approx 1{\cdot}8 \times 10^2\,\text{s}^{-1}$ which is in remarkable (possibly fortuitous) agreement with the measured value of $2 \times 10^2\,\text{s}^{-1}$.

The reluctance of the NaCl phonons to accept energy from vibrating CO is consistent with the large energy mismatch. At the NaCl transverse optical mode of $164\,\text{cm}^{-1}$ (Kittel 1986, Pireaux *et al.* 1985) 12 phonons need to be excited to accommodate the CO vibrational energy of $\tilde{\nu} \approx 1930\,\text{cm}^{-1}$. This then is expected to be an exceedingly inefficient relaxation process.

Guan *et al.* (1990) have explored CO on NaCl(100) in several models to examine the flow of vibrational energy. Unfortunately they use, as they admit, unrealistic parameters to describe the adsorbate surface interaction. As a consequence their estimate of $k_{\text{phn}} = 3 \times 10^{11}\,\text{s}^{-1}$ is orders of magnitude larger than either the experimental value of the fluorescence measurement or the theoretical value from the CPS model.

3.4. *Vibrational induced desorption rate*

The last relaxation channel to explore is the one that can lead to photodesorption. For the experimental measurement of this process, Chang and Ewing (1989) choose a cw rather than a pulsed laser source used in the fluorescence measurement of the preceding section. This avoids possible complications from non-linear effects that can accompany the high peak powers of a pulsed laser (Hess 1989, Harrison *et al.* 1988, Baldwin 1969). The principal exciting line of the laser source was $P_{1\to 0}(9)$ as before (see figure 15). The focusing optics for the laser beam directed it along the same path as the interrogating FTIR radiation shown in figure 4 while a beam block (not shown) protected the InSb detector. An area of $0{\cdot}1\,\text{cm}^2$ was bathed either by the laser or the FTIR radiation interrogating the monolayer before and after excitation. Use of geometric factors dictated by the optics and the cross-section of the monolayer at the laser frequency together with the source power of 10 mW yielded a pumping rate of

$k_p = 10\,s^{-1}$ (see (22)) from the $v=0$ to the $v=1$ level. The low power of the laser and relaxation to the substrate, at rate k_{phn}, prevented saturation of the $v=1$ level. Thus neither stimulated emission from the $v=1$ level nor up-pumping to higher levels is important. The experiment involved measuring the integrated absorbance change of the monolayer before excitation by the laser and after excitation for a time of $t=2\times10^4$ s (6 h). The absorbance change was negligible, as shown in figure 15. Nevertheless an upper limit was given to this change by the error in the absorbance measurement. With $\tilde{A}_p$, the integrated absorbance before excitation, and $\Delta\tilde{A}_p$, the error limit on the absorbance change, the fraction of molecules removed during the 6 h of excitation is given by $Y=\Delta\tilde{A}_p/\tilde{A}_p \leqslant 0{\cdot}06$. Analysis of the coupled equations of excitation and de-excitation ((15)–(17) and (22)) of the $v=1$ level and its depopulation by the variety of channels we have considered reveals

$$Y \approx k_{vid}k_p t/(k_p + k_{rad} + k_{phn}). \tag{25}$$

Using values of the rates already determined, we uncover $k_{vid} \leqslant 10^{-4}\,s^{-1}$. This rate implies a considerably less efficient desorption than found by Heidberg *et al.* (1987a) in pulsed laser excitation of CO on NaCl crystallites.

Why is this vibrational induced desorption rate so small and what are the factors that govern the rate k_{vid}? Lucas and Ewing (1981) modelled this relaxation channel for the general case A–$B^*\ldots S$ where A–B is a small molecule physisorbed to substrate S. We shall apply their model to CO*... NaCl in the calculation of the vibrational induced desorption rate. The initial state of the system is CO*... NaCl described by two quantum numbers: $v=1$ for the excitation of the chemical bond of CO and $v_z=0$ for the ground state of CO against its physisorbed bond to the surface of NaCl. Isoenergetic with this discrete state is the continuum of CO (now vibrationally relaxed in $v=0$) as it flies away with translational energy ΔE and velocity v from the surface of NaCl. This picture, which represents energy transfer from a discrete level into a continuum, invites application of the Golden Rule or its equivalent:

$$k_{vid} = (4/\hbar^2 v)|\langle\psi_f^{(0)}|V_c|\psi_i^{(0)}\rangle|^2. \tag{26}$$

In order to obtain k_{vid} it is needed to specify the final and initial state wavefunctions $\psi_f^{(0)}$ and $\psi_i^{(0)}$ and give the coupling term V_c.

Lucas and Ewing (1981) took the initial state wavefunction

$$\psi_i^{(0)} = R_{v_z}(z)\phi_1(\xi) \tag{27}$$

to describe A–$B^*\ldots S$, e.g. CO*... NaCl. The distance between the centre of mass of CO and the surface is given by the coordinate z as before. We can provide $R_{v_z}(z)$ which describes the vibration of CO against the surface only after the physisorbed potential is specified. Here the Morse potential was used

$$V(z) = D_e\{\exp[-2a(z-z_e)] - 2\exp[-a(z-z_e)]\}, \tag{28}$$

which is a slice of the full potential of (1). The steepness of the potential energy function is given by the range parameter a. The analytical form of the Morse oscillator wavefunctions are given elsewhere (Ewing 1978). For the initial surface bond mode we shall take $v_z=0$. An harmonic oscillator wavefunction $\phi_v(\xi)$ describes the internal vibrational displacement of CO against its chemical bond with initial state $v=1$.

The final state wavefunction

$$\psi_i^{(0)} = R_q(z)\phi_0(\xi) \tag{29}$$

defines $A–B+S$, e.g. CO + NaCl. The CO molecule has been released from the surface and is now vibrational relaxed so $v=0$. As CO flies far away from the surface with translational kinetic energy ΔE its wavefunction resembles a plane wave. Near the surface the translational motion of CO is moderated by its interaction with the surface. The wavefunction $R_q(z)$ describing the continuum behaviour of CO under the influence of the Morse potential is given elsewhere (Ewing 1978). Analogous to the quantum number v_z for the discrete state wavefunction $R_{v_z}(z)$ is the parameter q that describes the nodal behaviour of the continuum wavefunction $R_q(z)$. Later we shall treat q as an effective quantum number for the translational motion of CO. Fortunately we do not need the involved analytical forms of either $R_{v_z}(z)$ or $R_q(z)$ to calculate k_{vid}.

The coupling term V_c must connect the coordinates of the vibrating chemical bond, ξ, of CO with its surface bond, z. It is imagined that motion of the chemical bond of CO modulates the surface potential energy only because the distance between C and Na^+ changes. This form of the coupling term proposed many years ago for vibrational relaxation processes (Herzfeld and Litovitz 1959) is given by

$$V(z,\xi)=-2\gamma a D_e \xi\{\exp[-2a(z-z_e)]-\exp[-a(z-z_e)]\}, \tag{30}$$

where the fraction of displacement of C toward the (rigid) surface is

$$\gamma=m_o/\text{m} \tag{31}$$

with m_o the mass of the oxygen atom and m the mass of CO.

Fortunately the matrix element of the Golden Rule using the expression for the wavefunctions and the coupling term has a simple analytical result. The algebra yields

$$k_{\text{vid}}=4\pi^2\hbar^{-1}\gamma^2a^2\langle\xi\rangle^2D_e[(2d_o-2)!]^{-1}\left\{\prod_{n=1}^{d_o}[(n-\tfrac{1}{2})^2+q^2]\right\}$$
$$\times\{[(d_o-\tfrac{1}{2})^2+q^2]/2d_o^2\}\exp(-\pi q). \tag{32}$$

Several terms need defining in this rate expression. The harmonic oscillator matrix element for the adsorbate is

$$\langle\xi\rangle=\langle\phi_o(\xi)|\xi|\phi_1(\xi)\rangle=\hbar/(2\mu W)^{1/2}, \tag{33}$$

where μ is the CO reduced mass and W is its vibrational energy. The adsorbate trapped by the Morse potential can be represented by the dimensionless parameter

$$d=(2mD_e)^{1/2}/a\hbar. \tag{34}$$

Since the Morse parameters for the surface bond are not well known we lose little useful information by rounding off d to an integer and calling it d_o. This parameter which appears in the rate expression of (32) may be interpreted as the number of bound states of CO contained in the Morse potential well. The final translational energy ΔE of CO, now released from the surface, is incorporated into the dimensionless term

$$q=(2m\Delta E)^{1/2}/a\hbar=p/a\hbar, \tag{35}$$

which is momentum, p, scaled by the range parameter a. Since $\lambda=h/p$ the q parameter is related to the de Broglie wavelength of CO flying away from the surface. The parameter q appears in the rate expression of (32). We now have all the expressions needed to perform numerical calculations of k_{vid} for vibrational predissociation of the adsorbate on the surface.

For CO on NaCl(100), the energy gap is the difference between the vibrational energy of $^{13}C^{16}O$, $\tilde{\nu}=2107\,cm^{-1}$, and that needed to break the surface bond $\Delta E=\tilde{\nu}-D_0=600\,cm^{-1}$. The mass of CO is $m=29$ amu. The range parameter is difficult to estimate and a typical value is $a=2\times10^{10}\,m^{-1}$ (Ewing 1987) which gives $d_0=27$ from (34) and $q=16{\cdot}2$ from (35). Calculation of $\langle\xi\rangle=3{\cdot}3$ pm from the $^{13}C^{16}O$ molecular constants then enables (32) to be evaluated to give $k_{vid}=4\times10^{-3}\,s^{-1}$. This value is at least an order of magnitude larger than the measured rate. However, the calculated rate is exceedingly sensitive to the choice of the range parameter. Decreasing a by 10% ($a=1{\cdot}8\times10^{10}\,m^{-1}$) gives $k_{vid}\approx10^{-5}\,s^{-1}$ while an increase by 10% ($a=2{\cdot}2\times10^{10}\,m^{-1}$) yields $k_{vid}\approx10^{-2}\,s^{-1}$. Thus a 10% error in a corresponds to a swing in k_{vid} by three orders of magnitude. We can check on the reasonableness of these choices of a by calculating the value of $\tilde{\nu}_z$ they imply. Approximating the bottom of the Morse well as a harmonic potential it is easy to show that

$$\tilde{\nu}_z=a(2D_e/m)^{1/2}/2\pi c. \tag{36}$$

(Use of cgs units will assure that $\tilde{\nu}_z$ is in wavenumbers.) The values of a we have used give $\tilde{\nu}_z=112$ to $136\,cm^{-1}$, which is comparable to $\tilde{\nu}_z=90\,cm^{-1}$ estimated by Gevirzman *et al.* (1969) and consistent with the statistical mechanics analysis of section 2.3. In any event all these rates are exceedingly slow and encompass the experimental limit of $k_{vid}\leqslant10^{-4}\,s^{-1}$ provided by Chang and Ewing (1990a).

Why is k_{vid} so slow? We can answer this question by reducing (32) to the form of selection rules developed by Chang and Ewing (1989) and Ewing (1987). In order to better reveal the factors important for determining the magnitude of k_{vid}, (32) can by some severe approximations be cast into the form

$$k_{vid}\approx10^{13}\exp[-\pi(\Delta n_v+\Delta n_r+\Delta n_t+\Delta n_p)], \tag{37}$$

where $10^{13}\,s^{-1}$ gives the magnitude of the translational collision frequency ($\approx\tilde{\nu}_z c$) of the adsorbed molecule (e.g. CO) against the substrate (e.g. NaCl(100)). The argument of the exponent,

$$\Delta n_T=\Delta n_v+\Delta n_r+\Delta n_t+\Delta n_p, \tag{38}$$

gives the total change in quantum numbers during the relaxation process. Equation (37) states that the lifetime of the excited state, through this relaxation channel, depends exponentially on the total quantum change for the process. While values of k_{vid} resulting from the rate expression of this equation are quantitatively unreliable, the qualitative predictions provide understanding to both experimental results and involved theoretical calculations.

The individual quantum number changes in the exponential of (37) are $\Delta n_v\approx|\Delta v|$ for the change in vibrational state of the excited molecule during the relaxation process. For the relaxation of CO($v=1$)... NaCl(100), where CO($v=1$) desorbs to give CO($v=0$) we have $\Delta n_v\approx1$. This term in the exponential roughly accounts for $\gamma^2a^2\langle\xi\rangle^2$ in (32). The change in rotational state is given by Δn_r. If $\Delta n_r\approx0$, the product of desorption leaves the surface rotationally cold. The number of phonons within the substrate that are excited by the desorption process is roughly represented by Δn_p. Usually the biggest contribution to Δn_T is given by the translational quantum number change,

$$\Delta n_t\approx(d+q-2)/4. \tag{39}$$

Essentially (39) counts the number of nodes of the plane wave describing the relaxed molecule of mass m near the surface as it leaves with kinetic energy ΔE.

Returning to the question: why is k_{vid} so small for CO($v=1$)...NaCl(100)? The answer is because the total change in quantum numbers for the process is so large. For our example, with a generous uncertainty implied by (39), we have $\Delta n_t \approx 10 \pm 2$ and with $\Delta n_v \approx 1$ the total quantum change for the photodesorption process is $\Delta n_T \approx 11 \pm 2$. This provides a range of rates for k_{vid} that encompass the value of $4 \times 10^{-3}\,s^{-1}$ we calculated using the more cumbersome (32). Others by theoretical considerations have not found k_{vid} to be small for this system. Ben Ephraim *et al.* (1988) suggest an important role for rotations in the photodesorption process. However, this rotation-assisted channel is likely closed in the monolayer of coupled CO. Their estimate of k_{vid} differs 15 orders of magnitude from our measurement. Gortel *et al.* (1987) address the importance of Δn_p in their discussion of phonon-assisted desorption. Their estimate for k_{vid}, assuming similar values of the a parameter, is essentially in agreement with our result.

Muckerman and Uzer (1989) have explored the mechanism of vibrational induced desorption. In their 'van der Waals' model, the substrate was treated as rigid as was done by Lucas and Ewing (1981). They also choose a one-dimensional Morse potential to describe the surface bond. In applying their treatment to CO on NaCl(100), they arrive at an estimate of k_{vid} of the order of $10^{12}\,s^{-1}$. This value is at least 16 orders of magnitude faster than the experimental results of Chang and Ewing (1990a). The vast difference between the estimate we have just calculated for k_{vid} and that of Muckerman and Uzer (1989) is in the choice of the range parameter a. They have chosen $a = 17 \times 10^{10}\,m^{-1}$ which together with $D_e = 18\,kJ\,mol^{-1}$ implies a frequency against the surface of $\tilde{\nu}_z = 1050\,cm^{-1}$ by (36), or a factor of 10 higher than the frequency estimated by Gevirzman *et al.* (1969). In later papers Guan *et al.* (1990) have admitted that their choice of a is not reasonable. However, this value, yielding relaxation processes on the picosecond time scale, has allowed them to explore time evolution of the wave packet or classical trajectories. By considering a one-dimensional lattice of NaCl they have also explored the phonon relaxation channel. Their calculated value of k_{phn} is seven orders of magnitude faster than either the experimental result of Chang and Ewing (1990a) or the theoretical estimate by the CPS model (Chance *et al.* 1978). While the theoretical approach of Guan *et al.* (1990) provides insight into molecule-surface dynamics in general, their results add little to understanding the model CO*...NaCl(100) system because of their unreasonable choice of a.

4. Afterword

In this review of the structure and dynamics of CO on NaCl(100), we find a reasonable theoretical understanding of the data. The structure of the monolayer can largely be explained by ion produced electric fields directing the CO molecules over Na^+ on the NaCl(100) face. Attractions among the CO molecules in the monolayer are weak and the adsorption process is well represented by Langmuir isotherms. Vibrational relaxation into the substrate and through photodesorption has been experimentally measured and theoretically modelled. While vibrational dephasing processes are qualitatively understood, the successful treatment of collective motions in this relaxation channel is wanting. Collective vibrations can however account for a variety of spectroscopic features. With the study of the model system CO on NaCl(100) well under way, what of other related systems?

Consider first structural studies. Groups in Bloomington (Berg and Ewing 1989) and Hanover (Heidberg *et al.* 1990a–e) have explored the infrared spectroscopy of CO_2 on NaCl(100). Intermolecular interactions, in contrast to CO no NaCl(100), influence

the monolayer structure of CO_2. Preliminary spectroscopic work on C_2H_2 and CH_4 on NaCl(100) has also been reported (Berg *et al.* 1990). Finally, a structure for HBr on LiF(100) has been described (Blass *et al.* 1990). All these studies have relied on infrared spectroscopy to uncover monolayer structures on the alkali halides. Low energy electron diffraction (LEED) has also been applied to the alkali halide substrate (Barjenbruch *et al.* 1989) from which adlayer structures may be determined. Finally, low energy helium scattering from adsorbed molecules has been shown to be a promising technique for two-dimensional structure examinations (Jung *et al.* 1989). Each of these experimental probes of the monolayer reveals its own piece of information on the structure. A consistent picture of a structure which satisfies all of the experimental data will likely be guided by theoretical analysis of the energetics of various bonding possibilities expanding on techniques pioneered by Gevirzman *et al.* (1969).

We shall now extrapolate the vibrational dynamics measurements of CO on NaCl(100) to other systems. We are encouraged by the dramatic success of the CPS model to account for phonon relaxation. In order to compare this model to general systems, A–$B^*\ldots S$, we shall cast (24) into a more useful form using well known relationships (Chang and Ewing 1989) between k_{rad} and μ^{01}, the transition dipole, to obtain

$$k_{phn}=\frac{\eta\kappa|\mu^{01}|^2}{\hbar|\hat{\varepsilon}(\tilde{\nu})+1|^2 z_e^3}. \tag{40}$$

We shall take the value of the transition dipole for CO of $\mu^{01}=0{\cdot}1$ D ($3{\cdot}3\times10^{-31}$ Cm) given by Zumofen (1978) to be typical of many molecules. Using the optical constants for substrate S of LiF and NaCl (Palik 1985) and keeping $z_e=330$ pm, the phonon relaxation rates for vibrationally excited adsorbed oscillators A–B^* over a wide range of frequencies are calculated for (40) and plotted on figure 17. The circle, from the experiment of Chang and Ewing (1990a), is remarkably close to the theoretical curve for NaCl, with vibration to phonon relaxation rates of the order of $10^9\,s^{-1}$ on semiconductors (Guyot-Sionnest *et al.* 1990) and $10^{12}\,s^{-1}$ on metals (Beckerle *et al.* 1990), the relaxation by alkali halides is by comparison exceedingly slow. Only below $1000\,cm^{-1}$ when the substrate begins to absorb radiation (κ gets large) is phonon relaxation efficient. LiF is uniformly more effective in relaxing a vibrationally attached molecule than is NaCl essentially because this substrate has higher values of κ. The model of CPS is remarkable in its simplicity of concept and application. Furthermore it requires no knowledge of the bonding of the adsorbed molecule to its substrate. So far the test of the model is the single datum of figure 17. Clearly other systems need to be studied as well.

Now let us consider vibrational induced desorption for the general case of A–$B^*\ldots S$. In order to discuss the problem qualitatively we have plotted (37) on figure 18. The reluctance of vibrationally excited CO on NaCl(100) to desorb is consistent with the large quantum change, Δn_T, that must accompany this process. We showed that $\Delta n_T\approx11\pm1$ for this system. The rate for photodesorption can be increased by reducing Δn_T which in turn requires a reduction in Δn_t. Here (35) tells us this may be accomplished by reducing the mass of the adsorbate and/or its energy released on photo-desorption. Consider for example H_2 on NaCl(100). The strong electric fields at the surface are sufficient to induce a dipole in H_2 and allow its infrared absorption (Folman *et al.* 1972). Let us estimate its bond to the surface as $D_0\approx800\,cm^{-1}$ and with its vibrational frequency of $\tilde{\nu}=4160\,cm^{-1}$ we have $\Delta E\approx3360\,cm^{-1}$. With a typical

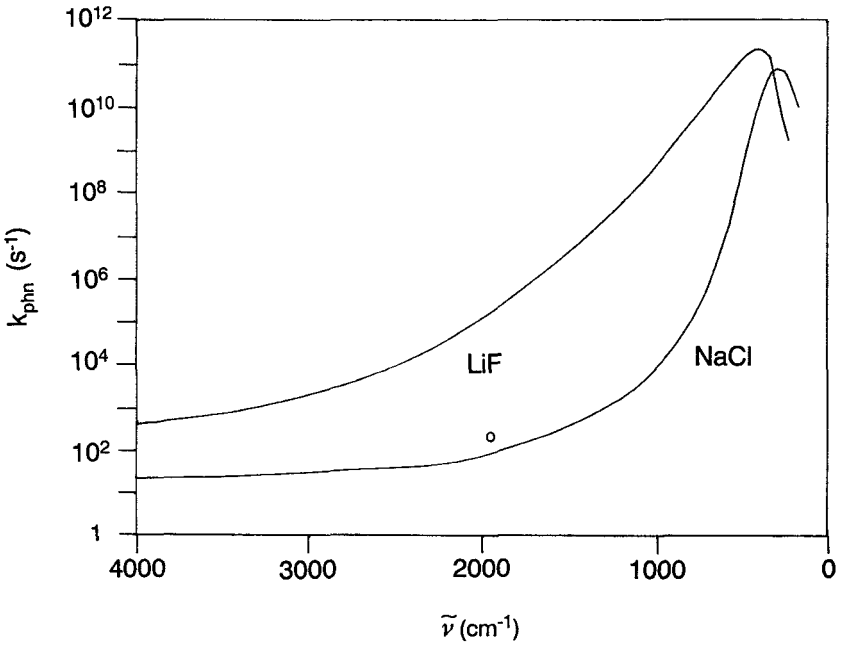

Figure 17. Phonon relaxation rates of A–B^*... S. The curves are from the theoretical model of Chance *et al.* (1978) using parameters given in the text. The vibrational frequency of A–B^* is $\tilde{\nu}$ and the substrate S is either NaCl or LiF. The circle is from experiments of CO*... NaCl(100) described in the text. From Chang and Ewing (1990c).

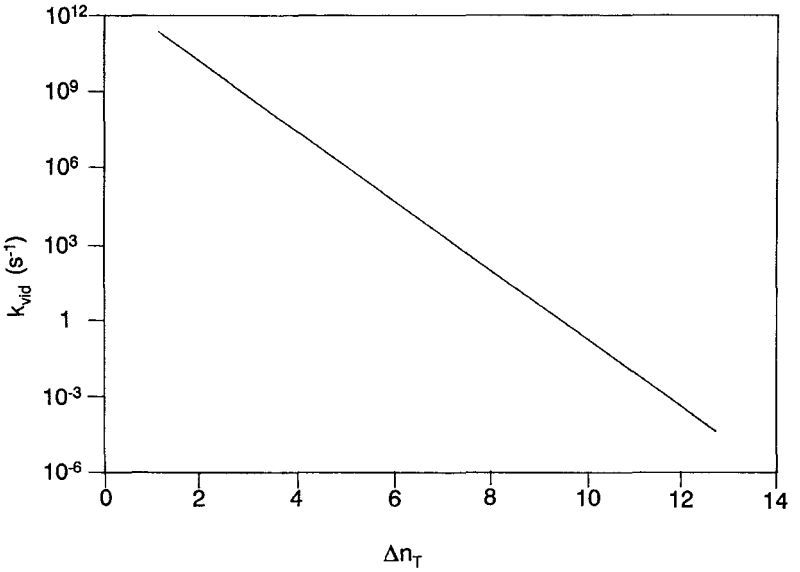

Figure 18. Vibrational induced desorption rates of A–B*... S. The total quantum change, Δn_T, for the desorption process is described in the text. Adapted from Chang and Ewing (1990c).

range parameter of $a = 2 \times 10^{10}\,\mathrm{m}^{-1}$ we arrive at $d = 5$ and $q = 10$ and $\Delta n_t \approx 3 \pm 1$ with $\Delta n_v \approx 1$ we have $\Delta n_T \approx 4 \pm 1$ or $k_{vid} \sim 10^{8\pm2}\,\mathrm{s}^{-1}$ from figure 18. The high frequency of H_2 is more than compensated by its light mass to reduce its momentum below that of CO. The integrated cross section for H_2... NaCl(100) is not known, but if we assume the value for CO... NaCl(100) figure 17 suggests $k_{phn} \sim 10\,\mathrm{s}^{-1}$. Variation of a and Δn_t by 30% still provides k_{vid} faster than k_{phn}. Thus we predict vibrationally induced desorption for $H_2(v=1)$... NaCl(100).

For polyatomic molecules on alkali halide surfaces, possibility for the photodesorbed product to carry away vibrational or rotational energy can have the effect of lowering the value of Δn_T, as Lucas *et al.* (1981) suggest. We consider CH_4 or its isotopes on NaCl(100) likely candidates for vibrationally induced desorption. Work on this system is in progress.

To our knowledge, all previous examples of vibrational desorption can be explained by surface heating (Heidberg *et al.* 1987b, Chuang 1983). The analysis we have just given suggests that certain systems should exhibit vibrational induced desorption.

An area of dynamics not yet represented by our model system involves electronic relaxation processes. Here we can imagine the photoexcitation of adsorbed CO on NaCl(100) and consider the flow of this energy as it is influenced by the substrate. Bond making or breaking, i.e. photochemistry, is a likely outcome of these experiments. Polanyi and Young (1990) have explored this interesting area using LiF(100) as the substrate with a variety of adsorbed molecules. The apparent success of the CPS model for vibrational relaxation suggests its application to questions of electronic relaxation as well. This has already been demonstrated for multilayer electronic relaxation (Chance *et al.* 1978).

By a thorough exploration of a model system, CO on NaCl(100), we have tried to offer some insight into general problems of surface structure and dynamics of other alkali halides. We hope to some extent to have been successful.

Acknowledgments

I thank Dr David Clary for the hospitality he has extended to me at Cambridge University where this review was written. I am grateful to Dr Nabil Amer for the prints of the AFM images of NaCl(100). The research I have described here is largely that of those who have worked with me: Hugh Richardson, Huan Chang, Robert Disselkamp and Chifuru Noda. I am fortunate to have learned so much from them. The National Science Foundation has generously supplied funds for this work.

References

ADAMSON, A. W., 1990, *Physical Chemistry of Surfaces*, 5th edition (New York: John Wiley).

AIRY, G. B., 1833, *Phil. Mag.*, **2**, 20.

AMOS, R. D., 1979, *Chem. Phys. Lett.*, **68**, 536.

BALDWIN, G. C., 1969, *An Introduction to Non-Linear Optics* (New York: Plenum).

BARJENBRUCH, U., FÖLSCK, S., and HENZLER, M., 1989, *Surf. Sci.*, **211/212**, 749.

BASSETT, G. A., 1958, *Phil. Mag.*, 1042; see also BETHGE, H., p. 201, in *Physics at Surfaces* by Zangwill, A., 1988 (Cambridge: Cambridge University Press).

BAUSCHLICHER, C. W. JR., 1985, *J. chem. Phys. Lett.*, **118**, 307.

BECKERLE, J. D., CASASSA, M. P., CAVANAGH, R. R., HEILWEIL, E. J., and STEPHENSON, J. C., 1990, *Phys. Rev. Lett.*, **64**, 2090.

BENEDEK, G., BRUSDEYLINS, G., DOAK, R., SKOFRONICK, J., and TOENNIES, P., 1983, *Phys. Rev.* B, **28**, 2104.

BEN EPHRAIM, A., FOLMAN, M., HEIDBERG, J., and MOISEYEV, N., 1988, *J. chem. Phys.*, **89,** 3840.
BENJAMIN, I., and REINHARDT, W. P., 1989, *J. chem. Phys.*, **90,** 7535.
BERG, O., and EWING, G. E., 1989, *Surf. Sci.*, **220,** 207.
BERG, O., QUATTROCCI, L., DUNN, K. S., and EWING, G. E., 1990, *J. Electron Spectrosc. and Rel. Phenom.*, **54/55,** 981.
BETHGE, H., 1965, *Surf. Sci.*, **3,** 33.
BLASS, P. M., JACKSON, R. C., POLANYI, J. C., and WEISS, H., 1990, *J. Electron Spectrosc. and Rel. Phenom.*, **54/55,** 993.
BORTOLANI, V., MARCH, N. H., and TOSI, M. P. (editors), 1990, *Interaction of Atoms and Molecules with Solid Surfaces* (New York: Plenum Press).
BRADSHAW, A., and SCHWEIZER, E., 1988, in *Spectroscopy of Surfaces*, edited by R. Clark and R. Hester (New York: Wiley).
CHABAL, Y. J., 1988, *Surf. Sci. Reports*, **8,** 211.
CHANCE, R. R., PROCK, A., and SILBEY, R., 1978, *Adv. chem. Phys.*, **37,** 1.
CHANG, H.-C., and EWING, G. E., 1989, *Chem. Phys.*, **139,** 55; 1990a, *Phys. Rev. Lett.*, **65,** 2125; 1990b, *J. phys. Chem.*, **94,** 7635; 1990c, *J. Electron Spectrosc. and Rel. Phenom.*, **54/55,** 39.
CHANG, H.-C., NODA, C., and EWING, G. E., 1990, *J. Vac. Sci. Tech.* A, **8,** 2644.
CHANG, H.-C., RICHARDSON, H. H., and EWING, G. E., 1988, *J. chem. Phys.*, **89,** 7561.
CHEN, W., and SCHAICH, W. L., 1989, *Surf. Sci.*, **218,** 580.
CHUANG, T. J., 1983, *J. Electron Spectrosc. and Rel. Phenom.*, **29,** 125.
CLAYTON, J. O., GIAUQUE, W. F., 1932, *J. Am. Chem. Soc.*, **54,** 2610.
CRAIG, D. P., and WALMSLEY, S. H., 1968, *Excitons in Molecular Crystals* (New York: Benjamin).
DISSELKAMP, R., CHANG, H.-C., and EWING, G. E., 1990, *Surf. Sci.*, **240,** 193.
ERLEY, W., and PERSSON, B. N. J., 1989, *Surf. Sci.*, **218,** 494.
ESTEL, J., HOINKES, H., KAARMANN, H., NAHR, H., and WILSCH, H., 1976, *Surf. Sci.*, **54,** 393.
EWING, G. E., 1978, *Chem. Phys.*, **29,** 253.
EWING, G. E., 1987, *J. Phys. Chem.*, **91,** 4662.
FOLMAN, M., and KOZIROVSKI, Y., 1972, *J. Colloid Interface Sci.*, **38,** 51.
FOWLER, P. W., and PYPER, N. C., 1985, *Proc. R. Soc.* A, **398,** 377.
FOWLER, P. W., and TOLE, P., 1988, *Surf. Sci.*, **197,** 457.
GADZUK, J. W., 1987, *Vibrational Spectroscopy of Molecules on Surfaces*, edited by J. T. Yates, Jr., and T. E. Madley (New York: Plenum), pp. 49–103.
GEVIRZMAN, R., KOZIROVSKI, Y., and FOLMAN, M., 1969, *Trans. Faraday Soc.*, **65,** 2206.
GIRARD, C., and GIRARDET, C., 1988, *Surf. Sci.*, **195,** 173.
GORTEL, Z. W., PIERCY, P., TESHIMA, R., and KREUZER, H. J., 1987, *Phys. Rev.* B, **36,** 3059.
GRAD, J., HERNANDEZ, G., and MUKAMEU, S., 1988, *Phys. Rev.* A, **37,** 3835.
GREADY, J. E., BACSKAY, G. B., and HUSH, N. S., 1978, *Chem. Phys.*, **31,** 375; 1978, *J. Chem. Soc. Faraday II*, **74,** 1430.
GUAN, Y., MUCKERMAN, J. T., and UZER, T., 1990, *J. chem. Phys.*, **93,** 4383, 4400.
GUYOT-SIONNEST, P., DUMAS, P., CHABAL, Y. J., and HIGASHI, G. S., 1990, *Phys. Rev. Lett.*, **64,** 2156.
HAMERS, J. S., HOUSTON, P. L., and MERRILL, R. P., 1990, *J. chem. Phys.*, **92,** 5661.
HAMMAKER, R. M., FRANCIS, S. A., and EISCHENS, R. P., 1965, *Spectrochim. Acta*, **21,** 1295.
HARDY, J. P., EWING, G. E., STABLES, R., and SIMPSON, C. J. S. M., 1985, *Surf. Sci.*, **159,** L474.
HARRIS, A. L., ROTHBERG, L., DUBOIS, L. H., LEVINOS, N. J., and DHAR, L., 1990, *Phys. Rev. Lett.*, **64,** 2086.
HARRIS, C. B., SHELBY, R. M., and CORNELIUS, P. A., 1977, *Phys. Rev. Lett.*, **38,** 1415.
HARRIS, C. B., SHELBY, R. M., and CORNELIUS, P. A., 1978, *Chem. Phys. Lett.*, **57,** 8.
HARRISON, I., POLANYI, J. C., and YOUNG, P. A., 1988, *J. Chem. Phys.*, **89,** 1475.
HEIDBERG, J., STAHMER, K.-W., STEIN, H., and WEISS, H., 1987a, *J. Electron Spectrosc.*, **45,** 87.
HEIDBERG, J., STEIN, H., and WEISS, H., 1987b, *Surf. Sci.*, **184,** L431.
HEIDBERG, J., KAMPSHOFF, E., KÜHNEMUTH, R., SCHÖNEKÄS, O., STEIN, H., and WEISS, H., 1990a, *Surf. Sci.*, **226,** L43; 1990b, *Bunsenges. Phys. Chem.*, **94,** 112; 1990c, *ibid.*, **94,** 118; 1990d, *ibid.* **94,** 124.
HEIDEBERG, J., KAMPSHOFF, E., KÜHNEMUTH, R., SCHÖNEKÄS, O., and SUHREN, M., 1990e, *J. Electron Specrrosc. and Related Phenom.*, **54/55,** 945.
HERZBERG, G., 1950, *Spectra of Diatomic Molecules* (Princeton: Van Norstrand).
HERZFELD, K., and LITOVITZ, T., 1959, *Absorption and Dispersion of Ultrasonic Waves* (New York: Academic).

HESS, P., editor, 1989, *Topics in Current Physics* (Berlin: Springer Verlag), vol. 47.
HILL, T. L., 1960, *Introduction to Statistical Mechanics* (Reading, MA: Addison-Wesley).
JUNG, D. R., CUI, J., FRANKL, D. R., KIM, H.-Y., and COLE, M. W., 1989, *Phys. Rev.* B, **40,** 11893.
KASHIKARA, Y., KIMURA, S., and HARADA, J., 1989, *Surf. Sci.*, **214,** 474.
KITTEL, C., 1986, *Introduction to Solid State Physics*, 6th edition (New York: Wiley).
LAMBERT, D. K., 1991, *J. chem. Phys.*, **94,** 133.
LANDOLT, H. H., and BÖRNSTEIN, R., 1955, *Atom-und Molekularphysik* 4. *Teil, Kristable*, (Berlin: Springer-Verlag).
LEGAY-SOMMAIRE, N., and LEGAY, F., 1980, *I.E.E.E. J. quant. Electron.*, **QE–16,** 308.
LENNARD-JONES, J. E., and DENT, B. M., 1928, *Trans. Faraday Soc.*, **24,** 92.
LUCAS, D., and EWING, G. E., 1981, *Chem. Phys.*, **58,** 385.
LUCCHESE, R. R., and TULLY, J. C., 1984, *J. chem. Phys.*, **80,** 3451.
MAHAN, G. D., and LUCAS, A. A., 1978, *J. chem. Phys.*, **68,** 1344.
MEYER, G., and AMER, N. M., 1990a, *Appl. Phys. Lett.*, **56,** 2100; 1990b, *Appl. Phys. Lett.*, **57,** 2089.
MILLIKAN, R. C., 1963, *J. chem. Phys.*, **38,** 2855.
MUCKERMAN, J. T., and UZER, T., 1989, *J. chem. Phys.*, **90,** 1968.
NITZAN, A., and TULLY, J. C., 1983, *J. chem. Phys.*, **78,** 3959.
NODA, C., and EWING, G. E., 1990, *Surf. Sci.*, **240,** 181.
NODA, C., RICHARDSON, H. H., and EWING, G. E., 1990, *J. chem. Phys.*, **92,** 2099.
PALIK, E. D., editor, 1985, *Handbook of Optical Constants of Solids* (New York: Academic Press).
PAULING, L., 1960, *The Nature of the Chemical Bond* (New York: Cornell University Press).
PENNER, S. S., 1959, *Quantitative Molecular Spectroscopy and Gas Emissivities* (Reading: Addison-Wesley).
PERSSON, B. N. J., and RYBERG, R., 1981, *Phys. Rev.* B, **24,** 6954.
PERSSON, B. N. J., and RYBERG, R., 1990, *Chem. Phys. Lett.*, **174,** 443.
PERSSON, B. N. J., HOFFMAN, F. M., and RYBERG, R., 1986, *Phys. Rev.* B, **34,** 2266.
PIREAUX, J. J., THIRY, P. A., and CAUDANO, R., 1985, *Surf. Sci.*, **162,** 132.
POLANYI, J. C., and YOUNG, P. A., 1990, *J. Chem. Phys.*, **93,** 3673 and references cited.
RAVAL, R., HAQ, S., HARRISON, M. A., BLYHOLDER, G., and KING, D. A., 1990, *Chem. Phys. Lett.*, **167,** 391.
RICHARDON, H. H., BAUMANN, C., and EWING, G. E., 1987a, *Surf. Sci.*, **185,** 15.
RICHARDSON, H. H., and EWING, G. E., 1987b, *J. phys. Chem.*, **91,** 5883.
RICHARDSON, H. H., CHANG, H.-C., NODA, C., and EWING, G. E., 1989, *Surf. Sci.*, **216,** 43.
RYBERG, R., 1989, *Adv. Chem. Phys.*, **76,** 1.
SHELBY, R. M., HARRIS, C. B., and CORNELIUS, P. A., 1979, *J. chem. Phys.*, **70,** 34.
SOMORJAI, G., 1981, *Chemistry in Two Dimensions: Surfaces* (Cornell: Ithaca).
STONE, A. J., 1985, *Mol. Phys.*, **56,** 1065.
STONE, A. J., and PRICE, S. L., 1988a, *J. phys. Chem.*, **92,** 3325.
STONE, A. J., and ALDERSTON, M., 1988b, *Mol. Phys.*, **56,** 1047.
VAN DER HOFF, B. M. E., and BENSON, G. C., 1953, *Can. J. Phys.*, **31,** 1087.
VARASANI, P., SARANGI, S., and QUANT, J., 1975, *Spectrosc. Radiative Transfer*, **15,** 473.
YANAGIHARA, T., and YOMOGITA, K., 1989, *Surf. Sci.*, **219,** 407.
ZANGWILL, A., 1989, *Physics at Surfaces*, (New York: Cambridge University Press).
ZECCHINA, A., SCARANO, D., and GARRONE, E., 1985, *Surf. Sci.*, **160,** 492.
ZUMOFEN, G., 1978, *J. Chem. Phys.*, **68,** 3747.